



TALLINN UNIVERSITY OF TECHNOLOGY

SCHOOL OF ENGINEERING

DEPARTMENT OF ELECTRICAL POWER ENGINEERING AND MECHATRONICS

# **DESIGN OF SATELLITE ASSISTED IOT SOIL IRRIGATION MONITORING SYSTEM**

## **SATELLIITSIDE TOEGA IOT PINNASE KASTMISE MONITOORIMISE SÜSTEEMI ARENDAMINE** MASTER THESIS

Student: Erkin Sahin

Student code: 194521MAHM

Supervisor: Mart Tamre, Professor at Department of  
Electrical Power Engineering and  
Mechatronics

Co-supervisor: Alar Kuusik, Senior Researcher at Thomas  
Johann Seebeck Department of Electronics

Tallinn 2021

(On the reverse side of title page)

## **AUTHOR'S DECLARATION**

Hereby I declare, that I have written this thesis independently.

No academic degree has been applied for based on this material. All works, major viewpoints and data of the other authors used in this thesis have been referenced.

"10" JUNE 2021

Author: Erkin Sahin

*/signature /*

Thesis is in accordance with terms and requirements

"....."..... 20....

Supervisor: .....

*/signature/*

Accepted for defence

".....".....20... .

Chairman of theses defence commission: .....

*/name and signature/*

## **Non-exclusive Licence for Publication and Reproduction of Graduation Thesis<sup>1</sup>**

I, Erkin Sahin (name of the author) (date of birth: 04/06/1994 ) hereby

1. grant Tallinn University of Technology (TalTech) a non-exclusive license for my thesis Design Of Satellite Assisted Iot Soil Irrigation Monitoring System,

*(title of the graduation thesis)*

supervised by Mart Tamre,

*(Supervisor's name)*

1.1 reproduced for the purposes of preservation and electronic publication, incl. to be entered in the digital collection of TalTech library until expiry of the term of copyright;

1.2 published via the web of TalTech, incl. to be entered in the digital collection of TalTech library until expiry of the term of copyright.

1.3 I am aware that the author also retains the rights specified in clause 1 of this license.

2. I confirm that granting the non-exclusive license does not infringe third persons' intellectual property rights, the rights arising from the Personal Data Protection Act or rights arising from other legislation.

---

<sup>1</sup> *Non-exclusive Licence for Publication and Reproduction of Graduation Thesis is not valid during the validity period of restriction on access, except the university's right to reproduce the thesis only for preservation purposes.*

\_\_\_\_\_ *(signature)*

\_\_\_\_\_ *(date)*

**DEPARTMENT OF ELECTRICAL POWER ENGINEERING AND MECHATRONICS**  
**THESIS TASK**

**Student:** Erkin Sahin, 194521MAHM(name, student code)

Study programme, MAHM02/18, Mechatronics (code and title)

main speciality: Mechatronics

Supervisor(s): Professor Mart Tamre, Director of MSc Mechatronics programme

Senior Researcher, Alar Kuusik, Tallinn University of Technology,

Thomas Johann Seebeck Department of Electronics

**Thesis topic:**

(in English) Design Of Satellite Assisted IoT Soil Irrigation Monitoring System

(in Estonian) Satelliitside Toega IoT Pinnase Kastmise Monitoorimise Süsteemi

Arendamine

**Thesis main objectives:**

1. Design of soil moisture sensor
2. Design of LoRa based sensor node PCB
3. Web platform which gives vegetation index and soil moisture level

**Thesis tasks and time schedule:**

No	Task	Month
1	Literature review and testing available sensors	December
2	Design of sensor and calculating power consumption	December
3	Testing the sensors and designing LoRa node	April
4	Web user interface development	April
5	Final unit test	May

**Language:** English **Deadline for submission of thesis:** "11" JUNE 2021

**Student:** Erkin Sahin "....."....."10" JUNE 2021  
*/signature/*

**Supervisor:** Mart Tamre ..... "10" JUNE 2021  
*/signature/*

**Co-supervisor:** Alar Kuusik ..... "10" JUNE 2021  
*/signature/*

**Head of study programme:** Mart Tamre ..... "10" JUNE 2021  
*/signature/*

## CONTENTS

ABSTRACT .....	8
RESÜMEE .....	9
1. INTRODUCTION .....	10
2. LITERATURE REVIEW .....	11
2.1 Remote sensing .....	11
2.2 Soil sensors .....	13
2.3 LPWAN .....	15
2.4 Objectives of the thesis .....	16
3. METHODS.....	18
3.1 Capacitive sensor .....	18
3.2 LoRa.....	19
3.2.1 Network architecture .....	19
3.2.2 LoRa modulation .....	20
3.2.3 LoRa transmission time .....	26
3.2.4 LoRa network layers.....	27
3.3 Vegetation indices.....	28
3.2.5 Normalized Difference Vegetation Index(NDVI).....	28
4. RESULTS.....	30
4.1 Moisture sensor.....	30
4.1.1 Sensor selection .....	30
4.1.2 Sensor testing setup .....	32
4.1.3 Sensor production .....	35
4.2 Sensor node.....	40
4.2.1 The parts selection .....	40
4.2.2 Sensor node tests .....	44
4.3 Web platform .....	49
5. DISCUSSION.....	51
6. CONCLUSION .....	53
7. KOKKUVÕTE EESTI KEELES .....	54
LIST OF REFERENCES .....	55
APPENDIX 1 .....	60
APPENDIX 2 .....	61

## TABLE OF FIGURES

Figure 1: Parallel plate capacitor[23] .....	18
Figure 2: Coplanar capacitor .....	18
Figure 3: Network topology[27].....	20
Figure 4:Up-chirp[32] .....	22
Figure 5:Down-chirp[32].....	22
Figure 6: LoRa packet structure .....	25
Figure 7: LoRa OSI network layers[28].....	27
Figure 8: NDVI example[35] .....	29
Figure 9: DF Robot capacitive moisture sensor[38].....	30
Figure 10: Pino-Tech SoilWatch 10[41] .....	31
Figure 11: Pino-Tech SoilWatch 10 circuit.....	31
Figure 12: Catnip electronics I2C moisture sensor .....	32
Figure 13: Dry soil sample weight .....	33
Figure 14: Weight of test samples when combined with sensor and water.....	33
Figure 15: Complete samples .....	33
Figure 16: Sensors' linear data fit .....	34
Figure 17: I2C sensor schematics.....	35
Figure 18: Sensor 3D model in KiCAD software.....	36
Figure 19: Panelized sensor in KiCAD software.....	36
Figure 20: Sensor programming setup.....	38
Figure 21: Mold design for the sensor .....	38
Figure 22: The sensor after final assembly.....	39
Figure 23: ESP32 Wrover-E module[45] .....	41
Figure 24: ESP32 Wrover-E block diagram[44] .....	41
Figure 25: Ra-02 LoRa radio module.....	42
Figure 26: Sensor node front view on KiCAD .....	42
Figure 27: Sensor node back view on KiCAD .....	42
Figure 28: Sensor node .....	43
Figure 29: Sensor node programmer 3D model(on left), and assembled programmer(on right) .....	43
Figure 30: Range test in Pirita tee .....	44

Figure 31: Battery level after one week of test.....	46
Figure 32: Sensor node and gateway location .....	46
Figure 33: Sensor node data flow .....	47
Figure 34: Sensor node assembly .....	48
Figure 35: Sensor node on the field.....	48
Figure 36:Moisture data on the map.....	49
Figure 37:NDVI data of TalTech campus area from Sentinel2 .....	49
Figure 38: Extracted region .....	50
Figure 39: NDVI and moisture levels on map.....	50

## **ABSTRACT**

The agricultural fields cover half of the food supply of the world. Being this huge industry also brings one of the most significant water consumption with it. Today the world's need for a clean water supply is in decline, and technology should reduce water consumption while monitoring the agricultural crop yield to keep as best as possible.

The research shows that monitoring soil moisture and satellite vegetation indices helps monitor soil health and crop yield. Thus, designing a system that monitors soil moisture levels and visualizes them with satellite vegetation indices could help monitor soil health and crop yield and reduce excessive watering in the agriculture field.

This thesis explains the design steps of such a system, shows validation of the system, and visualizes moisture data and vegetation indices on a map-based web platform.

## RESÜMEE

Põllumajandusmaa katab poole maailma toiduvarudest. See tohutu tööstusharu olemine toob endaga kaasa ka ühe märkimisväärseima veetarbimise. Täna väheneb maailma vajadus puhta veevarustuse järele ja tehnoloogia peaks veetarbimist vähendama, jälgides samal ajal põllumajanduskultuuride saagikust, et see oleks võimalikult hea.

Uuringud näitavad, et mulla niiskuse ja satelliittaimestiku indeksite jälgimine aitab jälgida mulla tervist ja saagikust. Seega võiks mulla niiskustaset jälgiva ja satelliittaimestiku indeksitega visualiseeriva süsteemi väljatöötamine aidata jälgida mulla tervist ja saagikust ning vähendada liigset kastmist põllumajanduse valdkonnas.

Selles lõputöös selgitatakse sellise süsteemi kavandamise etappe, näidatakse süsteemi valideerimist ning visualiseeritakse niiskuspõhiseid andmeid ja taimestikuindekseid kaardipõhisel veebiplatvormil.

# 1. INTRODUCTION

Today, agriculture directly covers 50 % of the world's survival needs[1]. While agriculture has a significant impact on food supply, it is also one of the considerable factors causing climate change. According to the Food and Agriculture Organization of the United Nations, in 2017, 541 000 000 tons of CO<sub>2</sub> emission was caused by agricultural operations, and the world 70 % of water withdrawal was caused by agriculture[1], [2]. Combined with improper waste management and misuse of chemicals, this withdrawn water is being filled with harmful toxins. Due to that, most fertile lands in the world having trouble to access to clean water.

Besides water problems, the agriculture industry is still catching up with new trends such as IoT and Industry 4.0. A smart agriculture solution could improve the sustainability, productivity, and resilience of a field. These smart agriculture systems could provide crop efficiency improvements by processing weather, soil moisture, soil pH, soil electrical conductivity, and satellite imagery of the land. While it may seem, the solution lies in the data processing, the hardware needed to collect this data plays a significant cost role.

While the mentioned metrics provides diagnostics about crops, a basic system compiled with a soil moisture sensor at various depth could give enough information about crop yields. It is possible to find various soil moisture sensors in the market but the components making it an Industry 4.0 and provides monitoring the field remotely sold at additional cost. In addition to the sensors, there are services where farmer could have information about the field via remote sensing. Remote sensing service providers offer surface moisture levels, vegetation index of specified field and weather data.

This thesis work is focused on an open-source agriculture solution that consists of a capacitive soil moisture sensor, a battery powered LoRa sensor node, a web platform where farmer can see the field with moisture levels and satellite vegetation indexes.

## 2. LITERATURE REVIEW

### 2.1 Remote sensing

There are remote sensing methods based on indexing satellite imaging. According to Lobell D.[3] satellite data could help simulate an experiment-based analysis of crop yield gap in the agriculture field. Lobell also mentioned how indexing improved by satellite image quality over time and gives examples of data loss resolution differences. The methods used for indexing according to Lobell et al. red, and near-infrared wavelength image-based vegetation indexing (VI) is the most straightforward and most efficient method. Early applications showed that these indexing applied to wheat and maize VI's can explain over 80 % of the observed crop yields. Later on, Lobell mentions the ratio of biomass to the total absorption of photosynthetically active radiation(PAR) as known as radiation use efficiency(RUE), was constant because plants adjust the leaf area and thus capture sunlight in response to other growth factors such as soil nutrients, water, and temperature stress. Lobell created a model for RUE and applied his model to MODIS data of wheat fields in Yaqui Valley, Mexico, and compared the yield gap results to other fields. Lobell pointed that remote sensing was becoming more widely available thanks to the cost and availability of satellite data increasing. He expressed that remote sensing will be a regular tool for agricultural analysts to assess yield gaps' magnitude and causes.

Another research from Berger A. et al. [4] showed the importance of the Normalized Difference Vegetation Index(NDVI) in terms of developing future prediction models based on historical satellite data. The study not only indicates satellite remote sensing in modelling but also includes ground sensors as well as drones. This study's primary objective explained the methodology's development and testing to estimate NDVI for the season. Berger et al. also showed that, MODIS data for NDVI for eight days at 250 m spatial resolution and more than 15 years of historical data. The study used seven different fields located in Brazil. Authors' approaches for modelling estimation includes two baseline time series of NDVI, for prediction quality evaluation with root-mean-square and parametric crop growth model which simulates on a daily time step the accumulation of biomass, biomass allocation, crop growth, leaf area development, light interception, water consumption, and water movement within the soil. The paper indicates, an RMSE of 8,88 % is obtained, considered all time-series of pixels included in the fields. The proposed procedure is compared with simple baseline forecast techniques, demonstrating improvements in quality and robustness. The quality of the best baseline was 10,72 % in the same conditions and with the worst standard deviation[4].

There is another study by Hatfield J. L. et al.[5] about spectral remote sensing to assist agronomics decisions. According to the article, the water-soluble pigment anthocyanins is an indicator of environmental stress, which could be caused by strong sunlight, UV-B-irradiation, low temperature, drought, wounding, bacterial and fungal infections, N and P deficiencies, herbicides, and pollutants[5]. As another material found in leaves are carotenoids, which have a structural role in the organization of photosynthetic membranes; participation in light-harvesting, energy transfer, quenching of chlorophyll excited states, and singlet oxygen; and interception of harmful free oxygen and organic radicals[5]. The study indicated that, the spectral response of accumulation of chlorophyll, carotenoids, and anthocyanin in leaves, as well as reflectance percentages of different wavelengths from dark green leaves to yellow leaves. According to the study, the standard deviation of wavelength based on chlorophyll level made peak at the green band -between 530 nm and 590 nm- and the red band at 710 nm. Hatfield et al. showed the spectral reflection relation of carotenoids and anthocyanin contents concerning chlorophyll levels.

A review paper about high accuracy soil moisture application based on satellite data conducted by Peng J. et al. gave existing applications of satellite-derived soil moisture products and identifies gaps between the characteristics of currently available soil moisture products and the application requirements from various disciplines[6]. In contrast, The data provided on paper was based on Advanced Scatterometer (ASCAT) onboard the Metop Satellites, the Advanced Microwave Scanning Radiometer2 (AMSR2), onboard the Global Change Observation Mission-Water (GCOM-W), the Soil Moisture and Ocean Salinity (SMOS) mission, and the Soil Moisture Active Passive (SMAP) mission[6]. Apart from these soil moisture products directly retrieved from single satellite platforms, merged 40 years of soil moisture products have been produced within the ESA CCI by harmonizing and combining multiple microwave-based soil moisture products[6]. According to Peng J. et al., recent soil moisture datasets usually have a coarse spatial resolution of about 25 km to 50 km. The challenge to increase spatial resolution can be solved with current and future satellite missions, such as the ESA Sentinel-1 European Radar Observatory, the Satélite Argentino de Observación COn Microondas (SAOCOM) mission, the NASA-ISRO Synthetic Aperture Radar (NISAR), the Radar Observing System for Europe L (ROSE-L), and the Tandem-L satellites, offer opportunities[6]. According to the study, the recent missions such as Copernicus Global Land Service and Sentinel-1 Mediterranean Soil Moisture could provide 1km spatial resolution. Besides soil moisture sensing, Peng J. et al. also included information about other application areas of current satellite systems: weather forecasting, climate modelling, hydrology, and hydrometeorological disasters.

## 2.2 Soil sensors

The one of the direct measurement methods could be using neutron probes. The neutron probes measure neutron fluxes caused by the interaction between secondary cosmic rays and hydrogen atoms[7]. Neutron probes use a radioactive source made from americium-beryllium to generate high-energy neutrons[8].

The research by Nguyen H. H. et al.[7] evaluated neutron probe-based soil moisture measurement system. The neutron probes were set to measure at certain depth levels as 10 cm, 20 cm, 30 cm, and 40 cm, and measurement has done hourly intervals according to authors. The results showed the probes are more sensitive first 10 cm soil layer so that quantifying the deeper layer in the ground-based soil moisture network tends to present a mismatch on the vertical scale[7]. According to Nguyen et al., the probes' measurement radiuses varied between 68 m and 157 m. and amongst the weighing methods used in the experiment, the linear measurement method provides more accurate data. While the study area characteristic of the experiment part of the paper is focused on evaluating linear depth weighing and non-linear depth weighing, sensor installation characteristics such as various depth measurements and weighing calculation radiuses showed that neutron probes are suitable for high resolution and precision soil moisture monitoring applications.

Another approach was based on RF backscattering. The device called Ground Penetrating Radar(GPR) uses RF backscattering to investigate dense mediums. While GPR applications can vary from metal detection to underground cave and sinkhole researches, it can also be used for soil moisture detection. The GPR for soil moisture sensing application can be a stationary setup[9] or a mobile setup[10] as well as an airborne setup[11].

The research concluded by Rice University and Microsoft proposed a Wi-Fi-based soil moisture level and soil electrical conductivity (EC) sensing. Initially, the author Ding J. et al.[9] suggested a GPR device that uses Time Domain Reflectometry(TDR); however, the broad application spectrum of GPR devices (from 100 MHz to GHz levels) is not available for unlicensed use. Since the 2,4 GHz spectrum is available for unlicensed use, the authors applied GPR methods to the 2,4 GHz spectrum. Ding J. et al. not only experimented with different depth measurements but also took moisture levels influences into account when measuring permittivity. The moisture level estimation in the paper used a previously trained model to extract moisture information from permittivity.

As a mobile application of GPR, Reza M., et al.[10] used off and on-ground GPR to map volumetric water content of the field. According to the authors, while the off-ground setup used a vectored network analyser (VNA) connected to 2 GHz TEM-horn antenna at the height of 1,1 m above the surface, the on-ground setup used a time-domain GPR system two transmitting (Tx) and receiving (Rx) 400 MHz bowtie with Tx and Rx offsets of 0,16 m and 1,26 m, respectively, thereby setting up a multi-offset system. The mapping was done by using VNA and a differential GPS. According to the results of the paper by Reza et al.[10] GPR could provide high precision measurements within a few meters of spatial resolution.

By creating an airborne GPR application, Kaijun w. et al.[11] showed how the drones help create sensing applications that classifies between local and remote. The authors used 700 MHz frequency for GPR. The most advantageous side of the application was replicating satellite remote sensing practises to a local scale by the drone's altitude control; a variable spatial resolution could be achieved. This provided scalable sensing applications by trading off the spatial resolution to sensing accuracy and vice versa, which results in a fast but coarse spatial resolution soil moisture mapping or slow but high-resolution sensing.

Another method used for moisture level sensing could be using a tensiometer. A tensiometer is comprised of a porous cup that allows water, but not air, to enter[12]. Water enters the tensiometer's evacuated ceramic cup until there is a hydraulic equilibrium between the soil water and the interior of the tensiometer. The equilibrium pressure, known as the matric pressure head, has been recorded using different devices, including manometers, burden gauges, and pressure transducers[13]. Because the tensiometer depends on osmosis forces of water, the measurement time compared to GPR slow, but the influence of salinity was not affecting the moisture level sensing. According to Mendes J. et al.[14] it is possible to reduce measurement time as low as 30 minutes by changing porous materials used in the tensiometer.

Another permittivity-based measurement method is based on measuring the dielectric constant( $\epsilon$ ) of the soil content. There are two approaches to this method capacitance measurement and direct EC measurement. In capacitance measurement, soil content acts as a variable capacitor as the soil media changes water levels, the capacitance changes. However, these changes are mostly in picofarad levels[15]. In direct EC measurement, the soil conductivity is measured. Compared to capacitance measurement, direct EC measurement uses exposed electrodes[16].

According to Deng X. et al.[15] capacitive soil moisture sensors require calibration depending on different soil types. However, it is possible to make a calibration-free

capacitive sensor by training a model with different soil content types, according to Deng et al. The authors propose a sensor made from a printed circuit board(PCB) with a specific shape. While PCB design resembles a parallel plate capacitor, authors simulate different shapes, plate gaps, and several electrodes because these factors play a major role in the sensor's range and sensitivity according to simulation results. The experiment was done with five different soil samples, with different loam and sand percentages. The proposed sensor offers 3,8 % accuracy, according to the authors.

A multifunctional soil probe designed by Valente A. et al.[16] offers soil moisture, EC, and thermal measurements. Valente et al. proposed a four aluminium electrode array arranged in the form of a Wenner array for EC measurement. However, volumetric water content was calculated by using temperature difference.

## **2.3 LPWAN**

The mentioned moisture level sensing approaches provide better spatial resolution than a satellite. Still, capacitive moisture sensing is best for cost-effectiveness within acceptable accuracy than the spatial resolution of satellite-based remote sensing. However, the data from the sensor still need to be collected. A low power wide area network(LPWAN) is the most suitable approach for such data collection operation.

NB-IoT is one of the LPWAN solutions in the market. Its standardization done by 3GPP. According to GSMA[17], NB-IoT aimed to provide a technology with high system capacity and a low minimum system bandwidth to facilitate its rollout. NB-IoT could provide download and upload speeds up to 200 kbps with 180 kHz bandwidth. It provides half-duplex communication up to 200 000 devices per cellular cell[17]. Currently, NB-IoT uses current cellular GSM and LTE networks in three different frequency allocation modes. Those modes could be:

- In-band mode: using frequencies which are occupied by LTE in LTE channel bandwidth,
- Guard band: It means using guard bands of an LTE channel,
- Standalone mode: This mode uses any available spectrum such as GSM.

Sigfox is another LPWAN. Unlike NB-IoT, Sigfox is a French company that uses the unlicensed Industrial Scientific Medical(ISM) spectrum -such as EU868- for communication. It uses differential binary phase-shift keying(DBPSK) and provides speeds up to 300 bps[18]. Since Sigfox is a commercial product, the owner company only offers a subscription-based business model. The current volume price for Sigfox modules is as low as 2\$. The target price was estimated to be as low as 0,2\$, with mass production[19]. A basic Sigfox subscription gives 144 uplink and four downlink messages per day. A Sigfox cellular cell can serve up to 50 000 devices[19]. Sigfox

provides a 10 km range in urban areas and a 40 km range in rural areas[20]. Sigfox collaborates with ETSI for standardization.

LoRa is another LPWAN designed by Semtech. Similar to Sigfox, LoRa also uses ISM band -such as 868 MHz, 915 MHz, and 433 MHz- and provides data rate up to 300 kbps[21]. Unlike Sigfox, LoRa uses chirp spread spectrum(CSS) and provides a 5 km range in urban areas and a 20 km range in rural areas. Even though a commercial entity developed LoRa compared to Sigfox, there is no subscription-based business model for LoRa; however, it is possible to use providers to register LoRa based devices for internet access. This registration requires a network layer called LoRaWAN. LoRa provides bidirectional communication in terms of no limitations on the downlink, which increases its application areas. The carrier-free side of LoRa makes local LoRa based LPWAN networks possible.

## **2.4 Objectives of the thesis**

While there are methods to collect soil moisture data remotely via satellite data, the resolution and data gathering time cannot be improved without extending and improving satellite networks. Therefore, a direct measurement method is required for high precision data. On the other hand, the satellite data is the fastest and cheapest way for vegetation indexing application.

According to the literature review given chapter 2.2, compared to satellite-based moisture level measurements, measuring soil moisture directly from soil gives better precision and more reliable data. However, not every mentioned method provides best solution in every case. To compare,

- Neutron probe requires a radioactive material which makes it dangerous to handle
- GPR requires a sophisticated antenna and processing power
- Tensiometer measurement takes time due to osmosis speed between soil and the device medium
- Permittivity based measurement methods provide an acceptable result but requires calibration for different soil types

Amongst the mentioned LPWAN methods, the key selection factor becomes energy efficiency, range and price. While most of them provides enough range for agricultural application, dependency to a central network could be a problem in remote locations. If compared, NB-IoT requires a service provider, therefore, a data plan, Sigfox costs the user for each message, on the other hand, LoRa could be set as a local network of as LoRaWAN with a carrier subscription plan or even a local LoRaWAN network where the network completely operated by the user.

The objectives of this thesis are:

- Designing a capacitive soil moisture sensor as a PCB for cost-effectiveness
- Designing a LoRa node connected to soil moisture sensor
- A web platform where user can interpret soil moisture data on the map as well as satellite images and vegetation indexes

### 3. METHODS

#### 3.1 Capacitive sensor

Capacitance is the amount of electrical charge a material can hold when the voltage is applied to it[22]. Commonly capacitors are visually represented as parallel plate capacitors and formulated as the ratio of charge to potential.

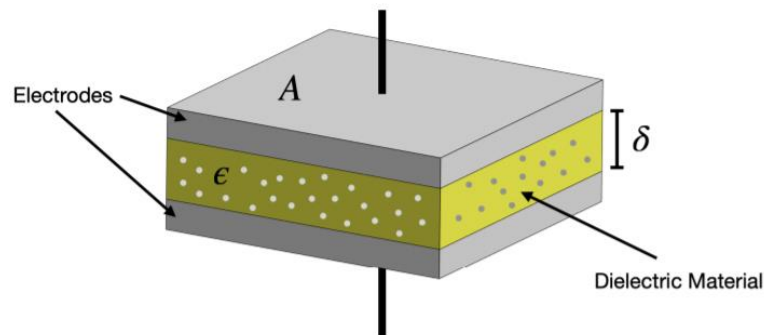


Figure 1: Parallel plate capacitor[23]

The ideal parallel plate capacitor requires the electric field to make a uniform path and uniform charge distribution between capacitor plates. This uniformity directly depends on the area, dielectric constant of the material, and distance between the plates.

While parallel plate representation gives an overview of the capacitor, to measure the influence of the surrounding medium rather than encapsulated material between plates, the coplanar capacitor gives the correct geometry.

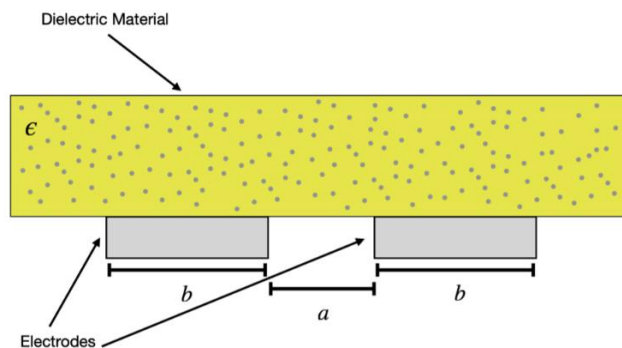


Figure 2: Coplanar capacitor

In a coplanar capacitor, the dielectric material is considered the material between exposed electrodes, thus measuring the material's dielectric constant.

The measurement of capacitance is mainly done by capacitance's effect on the known signal. It is done by combining the capacitor with other components in series or parallel, depending on the application.

In the scope of soil moisture measurement, the dielectric constant of the water is higher than in dry soil. To be more precise, while the dielectric constant of water is 80[24], the dry soil is between 2 to 6 [25]. The high permittivity allows electrons to flow better, thus increasing the capacitance.

## **3.2 LoRa**

LoRa is the abbreviation for "Long Range". LoRa is a wireless communication technology that uses LoRa Spread Spectrum technology with chirp modulation to achieve long-range radio communication with low power consumption. It has a frequency range between 137MHz to 1020 MHz. In the market, LoRa radios usually come with ISM(Industrial Scientific and Medical) Band variations which are 169 MHz, 433 MHz, 868 MHz, and 915 MHz[26]. While LoRa has long-range and low-power features, the trade-off comes from the data rate. The lower data range limits LoRa to perform for transmitting small packages for a short time. However, LoRa makes an ideal candidate for a moisture sensor application.

### **3.2.1 Network architecture**

The network components of a LoRa system consist of end nodes and gateways. In a basic setup, end nodes send data to the gateway, and data reaches a cloud system via the gateway. While the system can consist of many end nodes sending data to a gateway, it could also be many end nodes to many gateways that enable start-to-star topology.

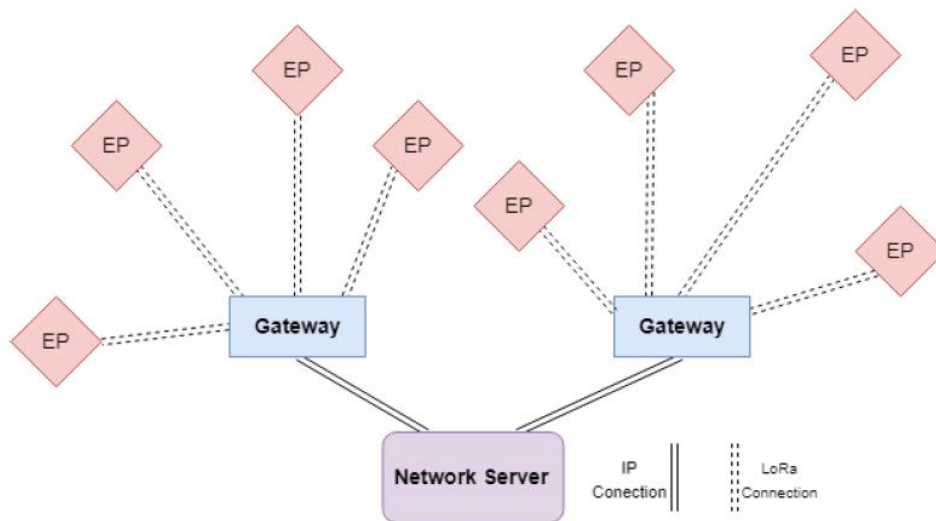


Figure 3: Network topology[27]

### 3.2.2 LoRa modulation

LoRa refers to the physical layer of LoRa radio developed by Semtech. LoRa modulation extends Chirp Spread Spectrum, which reduces energy consumption by transmitting data bits over the channel[26]. The data rate of the LoRa communication is calculated by the bandwidth in Hz, the spreading factor(SF), and the coding rate. Compared to Frequency Hopping, LoRa modulation has better immunity for interferences. According to Semtech, LoRa modulation can tolerate up to 30% with arbitrary power levels and symbol length with 6dB sensitivity degradation[28].

The spreading factor holds a significant role in communication quality, power consumption, and distance. The lower SF values provide a high data rate with low air time but limited communication distance. While higher SF values provide a more extended range, it comes with lower communication quality compared to lower values.

The spreading factor values in LoRa are between 7 to 12 with orthogonal communication, which allows communication of different networks in the same frequency without interference[26].

The signal-to-noise ratio (SNR) of different SF values can be seen in Table 1 below.

Spreading factor	Chirp/symbol	SNR of Demodulation
<b>7</b>	128	-7,5 dB
<b>8</b>	256	-10 dB
<b>9</b>	512	-12,5 dB
<b>10</b>	1024	-15 dB
<b>11</b>	2048	-17,5 dB
<b>12</b>	4096	-20 dB

Table 1: LoRa Spreading Factor values[21]

### Spread spectrum

The spread spectrum developed from the Shannon-Hartley theorem[29]. According to the Shannon-Hartley theorem, if the data transmitted at the rate of R on the channel a channel with higher bandwidth than R, reliable communication with a low SNR ratio can be achieved[29]. The Shannon-Hartley theorem provides the maximum achievable data rate of communication with the following formula[28], [30]:

$$C = B \left( \log_2 \left( 1 + \frac{S}{N} \right) \right) \quad (1)$$

Where C refers to channel capacity as bit per second, B is channel bandwidth in Hertz, S is average received signal power in bandwidth B, and N is noise on the channel. After the logarithm of base 2 to natural logarithm conversion following formula acquired[31]:

$$\frac{C}{B} = 1,433 \left( \frac{S}{N} \right) \quad (2)$$

In spread spectrum signal should be less than the noise floor. So it is safe to assume signal to noise ratio is less than 1. Which makes:

$$\frac{C}{B} \approx \frac{S}{N} \quad (3)$$

According to the equation for error-free transmission, bandwidth needs to be increased for the given channel with fixed SNR[30]

This method of increasing the bandwidth for lower noise levels called spread-spectrum. However, there are different approaches to the spread spectrum method.

## Chirp spread spectrum

One of the approaches is Chirp Spread Spectrum(CSS). A chirp signal is a sinusoidal signal which sweeps the frequency of the signal. The bandwidth of the chirp spread spectrum comes from the difference between start and end frequency. Depending on the sweep, the chirp signal is called up-chirp and down-chirp, where up-chirp has an increasing frequency and down-chirp has a decreasing frequency. The frequency change could be a linear change or an exponential change depending on the application[30].

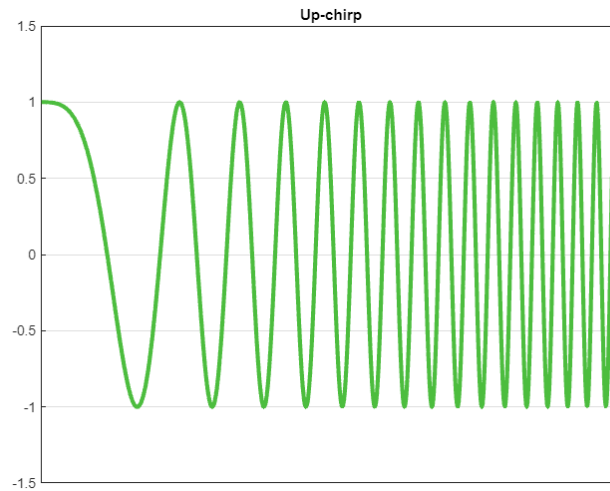


Figure 4:Up-chirp[32]

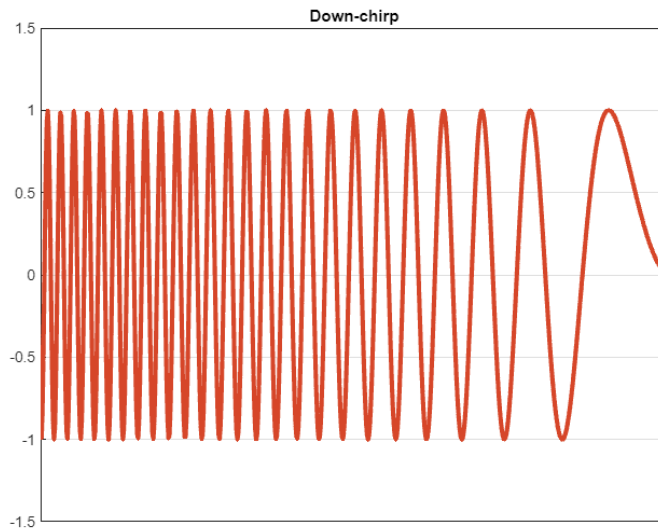


Figure 5:Down-chirp[32]

A sinusoidal signal is used to create a chirp signal[31], [32].

$$x(t) = A\cos(\omega_0 t + \phi) \quad (4)$$

Where A is amplitude. The equation can al be rewritten as the function of instantaneous phase[31], [32]

$$x(t) = A\cos(\theta(t)) = A\cos(\omega_0 t + \phi) = A\cos(2\pi f_0 t + \phi) \quad (5)$$

Where  $\theta(t) = \omega_0 t + \phi$  is the linear part of the sinusoid signal and its instantaneous phase. The angular frequency of the sinusoidal signal equals to the derivative of the instantaneous phase[31], [32]

$$\omega_0 = \frac{d}{dt}\theta(t) \quad (6)$$

In quadratic form[32]:

$$\theta(t) = 2\pi\alpha t^2 + 2\pi f_0 t + \phi \quad (7)$$

Where  $\alpha$  is constant. Therefore, the chirp signal takes the form of the following equation[32]:

$$x(t) = A\cos(\theta(t)) = A\cos(2\pi\alpha t^2 + 2\pi f_0 t + \phi) \quad (8)$$

For the sweeping part, the frequency in Hertz is[32]:

$$f_i(t) = 2\alpha t + f_0 \quad (9)$$

In a certain time duration, the rate of change in frequency[32]:

$$k = 2\alpha = \frac{f_1 - f_0}{T} \quad (10)$$

Where  $f_0$  is stat frequency of the sweep and  $f_1$  is the end frequency for  $T$ . When the equation substituted[32]:

$$\omega_i(t) = \frac{d}{dt}\theta(t) = 2\pi(kt + f_0) \quad (11)$$

$$\theta(t) = \int \omega_i(t)dt \quad (12)$$

$$= 2\pi \int (kt + f_0) dt = 2\pi \left( \frac{kt^2}{2} + f_0 t \right) + \phi_0 \quad (13)$$

$$= 2\pi \left( \frac{kt^2}{2} + f_0 t \right) + \phi_0 = 2\pi \left( \frac{kt}{2} + f_0 \right) t + \phi_0 \quad (14)$$

where  $\phi_0$  is the initial phase of the sweep as constant. Thus, the chirp generation equation becomes[32]:

$$x(t) = A \cos(\theta(t)) = A \cos(2\pi f(t)t + \phi_0) \quad (15)$$

Where the time-varying frequency function is[32]:

$$f(t) = \frac{k}{2}t + f_0 \quad (16)$$

### LoRa chirp

While many legacy wireless communication systems benefit from FSK for low energy consumption with high efficiency, LoRa uses a derived version of the Chirp Spread Spectrum. LoRa features variable data rate, utilization of orthogonal spreading factors. These features enable to trade data rate for range or power[28]. The features of LoRa CSS

In LoRa, the chirp bandwidth is equal to the signal. Therefore, the signal initially separated using a higher frequency signal, and then the signal is modulated as a chirp signal[28].

The bitrate of this modulation expressed as[28]:

$$R_b = SF \times \frac{1}{T_s} \quad (17)$$

$$T_s = \frac{2^{SF}}{BW} \quad (18)$$

Where the  $R_b$  is the bits per second, SF is the spreading factor, BW is the bandwidth of the modulated signal in Hertz and  $T_s$  is the symbol period in seconds.

As seen in the equation, the bit rate and the symbol period are inversely proportional. Therefore, the chip rate of LoRa represented as[28]:

$$R_c = R_s \times 2^{SF} \quad (19)$$

Where  $R_c$  is the chip rate,  $R_s$  symbol rate. While the symbol rate is inversely proportional to the symbol period, the equation for  $R_b$  becomes the following[28]:

$$R_s = \frac{1}{T_s} = \frac{BW}{2^{SF}} \quad (20)$$

$$R_c = \frac{BW}{2^{SF}} \times 2^{SF} \quad (21)$$

## LoRa packet

A standard LoRa packet consists of preamble symbols, header symbols, the payload, and payload CRC(Cyclic Redundancy Check).

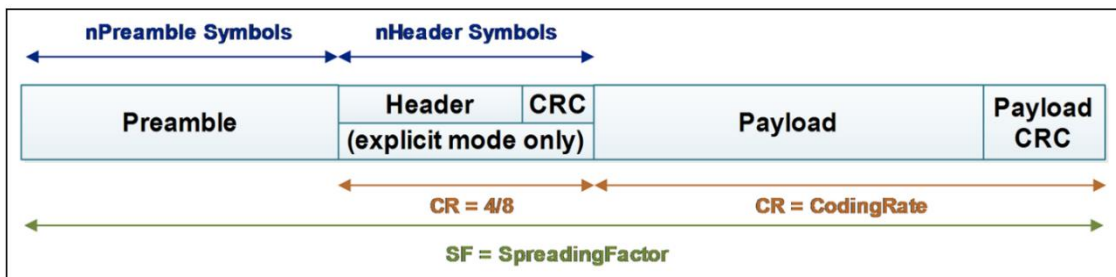


Figure 6: LoRa packet structure[33]

The preamble allows the receiver to synchronize for the incoming data, followed by an optional header. The header enables adjusting the coding rate besides containing the packet length information and whether the payload contains 16-bit CRC. While LoRa preamble can take a length between 10 to 65540 symbols, the payload data size is stored in single-byte, and the total payload limit is 255 bytes, giving enough space for communication[28].

The optional header-only is included in the explicit mode, where the header contains data of payload size, error correction code, and CRC mode[20]. In implicit mode, the header is not included; therefore LoRa packet is shorter. This short packet results in less air time than explicit mode making implicit more suitable to low-power applications. However, even the packet is not sent with a header; a LoRa packet still requires a header. In implicit mode, this header is preconfigured on both receiver and transmitter sides[28].

### 3.2.3 LoRa transmission time

The power consumption of LoRa communication depended on the combination of transmission time and LoRa radio power level. In addition, the transmission air time is affected by coding rate, spreading factor, and bandwidth.

According to Semtech, the transmission air time of LoRa calculated by the following steps[28]:

- The preamble transmission time calculated[28]

$$T_{preamble} = (n_{preamble} + 4.25)T_s \quad (22)$$

Where  $T_{preamble}$  preamble time,  $n_{preamble}$  is preamble symbol length, and  $T_s$  preamble symbol rate

- After the preamble, the transmission air time for the payload is calculated. Compared to preamble transmission air time, the payload transmission air time depends on symbols and payload length. However, maximum payload time is considered for the calculation[28]

$$EXPLICITn_{payload} = 8 + \left( \left( \frac{2P + 4CRC - SF + 7}{SF - 2D} \right) \times (CR + 4) \right) \quad (23)$$

$$IMPLICITn_{payload} = 8 + \left( \left( \frac{2P + 4CRC - SF + 2}{SF - 2D} \right) \times (CR + 4) \right) \quad (24)$$

Where SF is the spreading factor, D indicates whether the data rate optimization is enabled or not, CR is the coding rate for error-correcting, CRC is CRC enable indicator, and P is payload bytes.

The payload transmission duration is calculated from the product of payload symbol length and symbol rate[28].

$$T_{payload} = n_{payload} \times T_s \quad (25)$$

The total LoRa packet transmission time is the combination of payload and preamble times[28]:

$$T_{packet} = T_{payload} + T_{preamble} \quad (26)$$

### 3.2.4 LoRa network layers

LoRa is implemented as a physical layer by Semtech[28]. The physical layer benefits translation of the LoRa packet to data by the integrated circuit itself, providing rapid application development on top of the LoRa physical layer. The LoRa network is represented by Open Systems Interconnection (OSI) model. OSI model is a standard for different computer systems to be able to communicate with each other. Its is represented as a stack of communication system into seven abstract layers[34]. While the LoRa being a physical layer, it helps to integrate different applications to various systems, making the LoRa a good choice for long-range, low-power Internet of Things(IoT) applications.

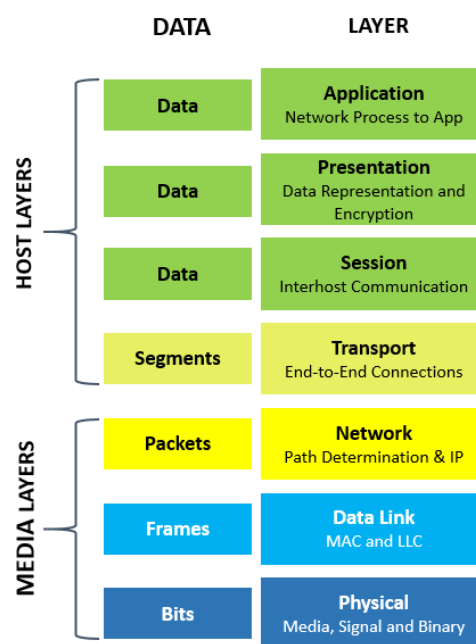


Figure 7: LoRa OSI network layers[28]

### 3.3 Vegetation indices

Vegetation indexes provide sensitive vegetation characteristics while minimizing the soil background, reflectance, and atmospheric effect factors[35]., The reflectance of near-infrared and visible light needs to be observed to determine green area density on the part of the land. When sunlight hits the objects, specific wavelengths are absorbed, and others are reflected. The pigment in plant leaves, chlorophyll, strongly absorbs visible light (from 0.4 to 0.7  $\mu\text{m}$ ) for photosynthesis[36]. The cell structure of the leaves, on the other hand, strongly reflects near-infrared light (from 0.7 to 1.1  $\mu\text{m}$ )[36]. Therefore more green leaves the plans have, the more light is reflected in specific wavelengths. This greenness is used as a vegetation index. The vegetation indexes give a ratio or difference of green with respect to soil. The most common vegetation index used is the Normalized Difference Vegetation Index(NDVI).

#### 3.2.5 Normalized Difference Vegetation Index(NDVI)

The NDVI is an indicator of the greenness of the biomes[37]; even though it is not a physical property of the vegetation cover, it is a straightforward formulation[37], [38].

$$NDVI = \frac{REF_{nir} - REF_{red}}{REF_{nir} + REF_{red}} \quad (27)$$

Where  $REF_{nir}$  is spectral reflectance in near-infrared waveband and  $REF_{red}$  is spectral reflectance of the red waveband.

As shown in Figure8, reflectance is given for green leaves as 50% in near-infrared and 8% in visible red light; for yellow leaves, 40% near-infrared and 30% in visible red light.

When NDVI applied to green leaves:

$$NDVI = \frac{REF_{nir} - REF_{red}}{REF_{nir} + REF_{red}} = \frac{0.5 - 0.08}{0.5 + 0.08} = 0.72 \quad (28)$$

For yellow leaves:

$$NDVI = \frac{REF_{nir} - REF_{red}}{REF_{nir} + REF_{red}} = \frac{0.4 - 0.3}{0.4 + 0.3} = 0.14 \quad (29)$$

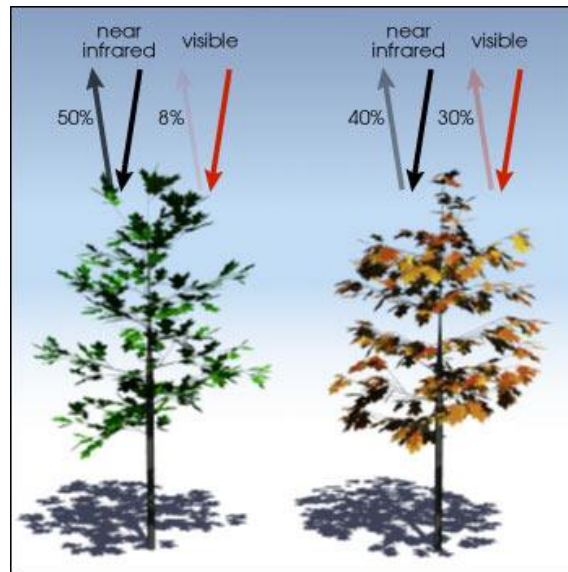


Figure 8: NDVI example[36]

According to the results, the green leaves have a higher value in NDVI compared to yellow leaves. While in this example comparison between green and yellow leaves made, it can also be applied to a part of the land where the difference between soil and green leaves can provide crop growth and yield data over a specific period.

## 4. RESULTS

This thesis's result is a system consisting of soil moisture and temperature sensor connected to a cloud service via the LoRa radio and a web platform where moisture data and NDVI are represented on the map. During the design phase of the system, three different moisture sensors were tested. The LoRa node and the gateway designed to be low-cost and low-power. The web platform is made as a map where users can put moisture, temperature, and NDVI data as layers on top of the map.

### 4.1 Moisture sensor

#### 4.1.1 Sensor selection

The final system consists of three identical sensors placed at 30cm, 60cm, and 90cm depth from the surface. These levels are chosen to determine the water flow characteristics of the soil, which can be used to provide predictions for the surface to root time of water. This metric would also benefit from predicting the fertilizers' travel time from surface to roots.

Three different sensors were tested for this system. The tests aimed to find a sensor that is low cost and accurate on the measurements.

#### The sensors

The first sensor was the DF Robot Capacitive Soil Moisture Sensor 1.2. It is the cheapest sensor amongst others, pricing at 5,16€[39].



Figure 9: DF Robot capacitive moisture sensor[39]

It uses a TLC555CDR timer IC[40] for a maximum 2.1MHz of clock source[41] and provides analog output between 1,2 Volts and 5,5 Volts[40]. The sensor comes with a 20cm cable. However, the system needs a longer cable. Even though the sensor works

stable with a given cable, when the cable length is extended, the sensor's voltage output started to fluctuate due to the resistance of the cable.

The second sensor was Pino-Tech SoilWatch 10, pricing at 26,90€[42].



Figure 10: Pino-Tech SoilWatch 10[42]

The sensor comes with a fixed cable length adjustable at the order. The sensor provided good results. However, its price makes it the most expensive sensor amongst others. Since the top part of the PCB is over-molded, it is impossible to determine the components of the device. When the molded plastic cut off, the components revealed similar circuitry of the DF Robot branded sensor instead of discrete components as 555 timer; the circuit is built by generic components. According to the manufacturer's datasheet sensor works at 75 MHz and provides analog output between 0 Volts and 3.3 Volts[43].



Figure 11: Pino-Tech SoilWatch 10 circuit

The third sensor is the Catnip Electronics I2C moisture sensor, priced at 10,96€[44]. This sensor differs from others in its communication system. While other sensors give analog output, this sensor provides data through the I2C bus. However, on the sensor, the moisture level measured as an analog value then forwarded via I2C.

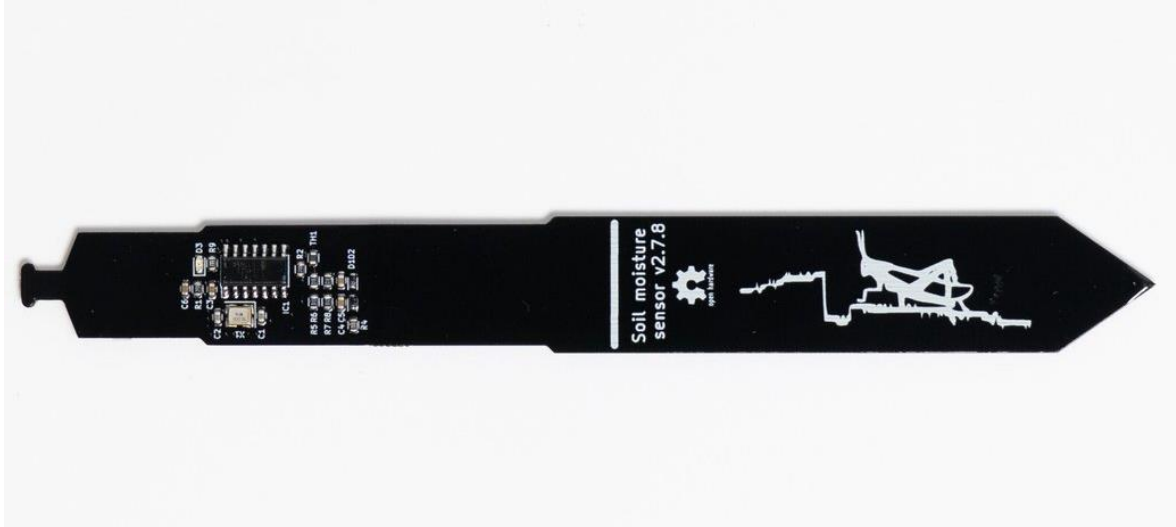


Figure 12: Catnip electronics I2C moisture sensor

Compared to other sensors, the I2C moisture sensor is equipped with a temperature sensor and light sensor.

#### 4.1.2 Sensor testing setup

The setup was prepared in three different containers with the same soil sample. The soil sample was taken from the TalTech soccer field, where the final installation was done. The separate containers were used because sensors might affect each other during sensing. For each sample, the soil dried completely then sensors were placed. The test is done in a closed room with 23,5°C average room temperature to create a controlled testing environment. The test aimed to collect the sensors' gravimetric moisture responses individually to compare their performance within the combination of other features. Each sample filled with 170g of dry soil sample then filled with 180g of water.



Figure 13: Dry soil sample weight



Figure 14: Weight of test samples when combined with sensor and water

In order to collect the data as a microcontroller, the ESP32-Wrover-E was used. Sampling period set to 12 hours and testing duration was 1 week.



Figure 15: Complete samples

The moisture levels are calculated in percentages according to maximum and minimum values of ADC and I2C data, where the maximum is the sensor is submerged to water thoroughly, and the minimum is the sensor is in the air.

	DF Robot	Pino-Tech	I2C sensor
Air measurement	155	243	398
Water submerged	713	850	788
Range	558	607	390

Table 2: Sensor range and min-max values

As seen in Table 2, the ADC sensors have more range compared to the I2C sensor. However, from the reliability perspective, the I2C sensor is the best since ADC sensors can easily be influenced by the surrounding environment as well as cable length.

	DF Robot		Pino-Tech		I2C sensor	
	Weight(g)	Level(%)	Weight(g)	Level(%)	Weight(g)	Level(%)
Interval 1	419	87	439	90	429	95
Interval 2	409	80	412	82	413	89
Interval 3	398	82	411	80	408	86
Interval 4	391	75	397	69	401	80
Interval 5	386	70	395	65	395	74
Interval 6	380	68	383	54	391	73
Interval 7	374	65	378	50	385	69
Interval 8	372	65	377	42	379	65
Interval 9	364	63	370	40	370	53
Interval 10	356	52	359	38	365	50
Interval 11	348	50	368	35	358	49
Interval 12	346	50	360	33	355	49
Interval 13	342	50	358	34	352	45
Interval 14	337	45	340	30	347	40

Table 3: 1 week of testing results

When the data recorded in Table 2 fitted in a chart in Figure 16, the sensor values seem similar. However, DF robot and Pino-Tech sensors have less  $R^2$  value than I2C sensor, making the I2C sensor the strongest in data reliability.

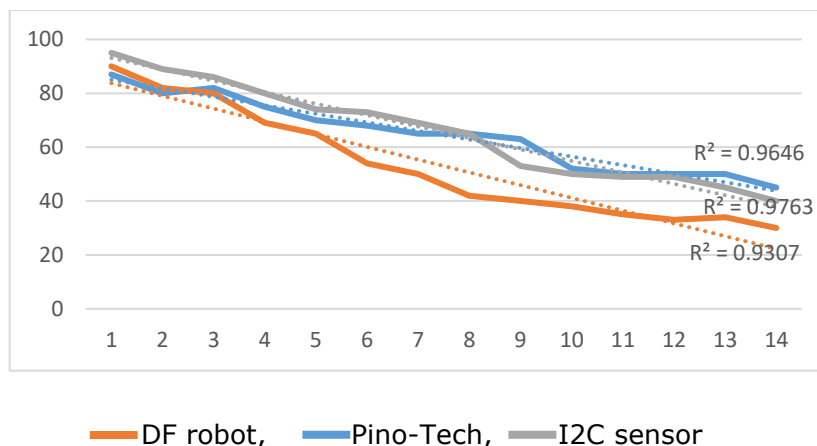


Figure 16: Sensors' linear data fit



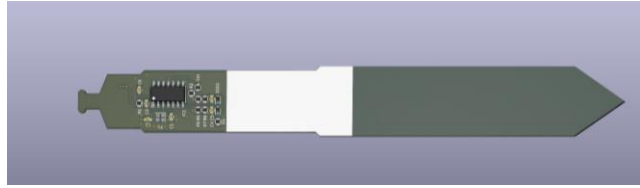


Figure 18: Sensor 3D model in KiCAD software

- PCB is panelized to reduce surface mount assembly costs. The single panel consists of 5 sensors

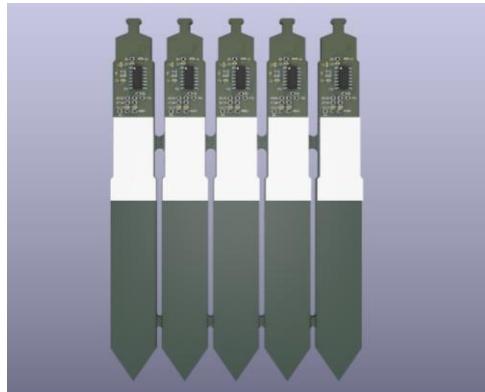


Figure 19: Panelized sensor in KiCAD software

The final material cost for 75 sensors can be seen in Table4.

Cost tag	Price (the exchange rate is 0,8238 at 19/01/2021)
PCB panel(15 pieces)	55,70
SMT assembly and parts	138,53\$
Shipping	24,67\$
Import tax	43,78\$
Total	262,68\$
Single sensor	3,5\$≈2,88€

Table 4: Sensor cost table

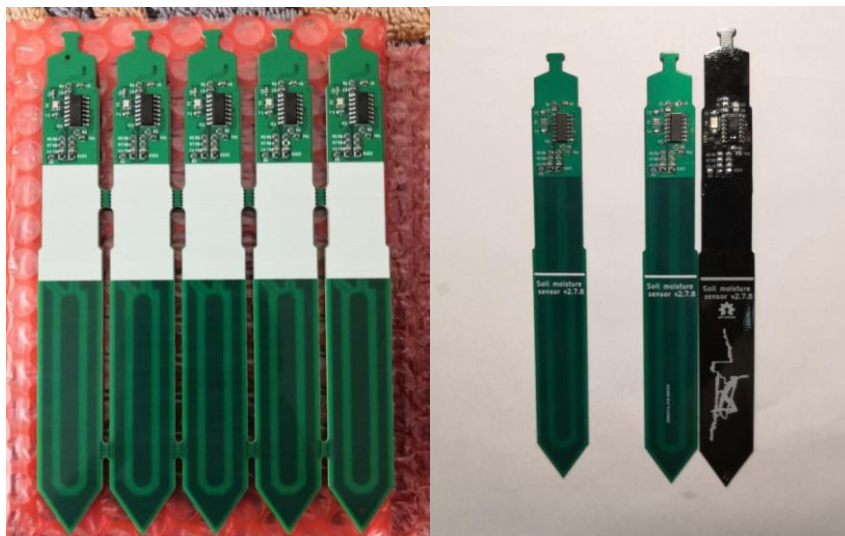


Table 5: Sensor panel and comparison to Catnip Electronics version

The re-produced sensor tested and compared the Catnip Electronics' sensor by using same test setup used in comparison of three sensors.

	Catnip Electronics		Re-produced I2C sensor	
	Weight(g)	Level(%)	Weight(g)	Level(%)
Interval 1	429	89	439	89
Interval 2	419	81	422	82
Interval 3	405	78	414	77
Interval 4	398	75	406	74
Interval 5	390	70	398	68
Interval 6	382	62	391	64
Interval 7	374	58	378	56
Interval 8	372	57	377	54
Interval 9	364	53	370	49
Interval 10	357	46	369	49
Interval 11	349	41	367	47
Interval 12	346	40	360	42
Interval 13	340	38	358	41
Interval 14	337	35	340	36

Table 6: Manufactured sensor comparison to the original design

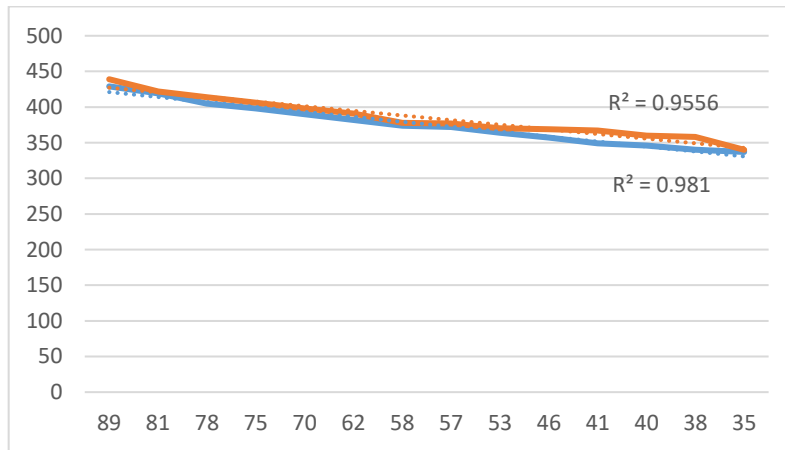


Table 7: Graph of Catnip Electronics and manufactured sensor

According to the linear regressions of sensors tested in Table 6, both sensors has similar responses. It is correct to assume that the design changes and manufacturing process did not change the sensor response drastically.

The original Catnip Electronics I2C Moisture Sensor software was used in the reproduced version of the sensor. In the tests, I2C sensors address set as follows: 0x20, 0x21, 0x22. However, a sensor programming fixture was designed to program sensors faster. The fixture has six spring-loaded contacts to provide a firm connection between the programmer and the sensor.



Figure 20: Sensor programming setup

The sensor electronics are covered with hot glue to provide waterproof coating and mechanical durability during the installation of the soil. A mold was created to provide a uniform and thick silicone layer coating, and silicone is applied to the sensor with cable assembly. The silicone layer thickness was designed to be 3mm.

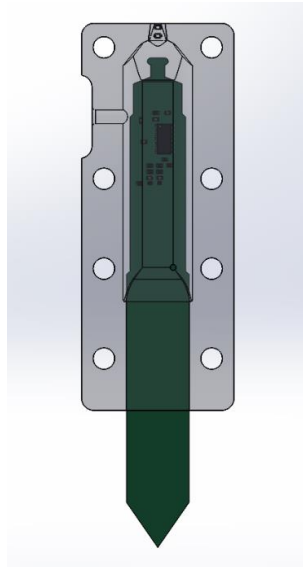


Figure 21: Mold design for the sensor

The sensor cable is the four-string telephone cable, and the end connector is the RJ-12 telephone connector. The connector was chosen to be easy to terminate and crimp.

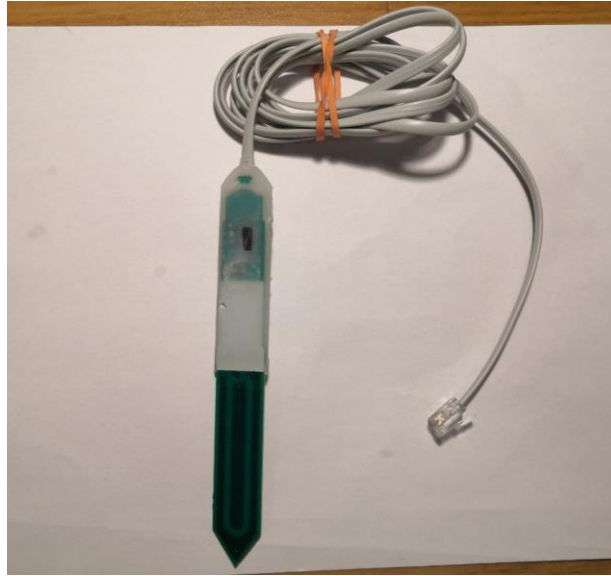


Figure 22: The sensor after final assembly

## 4.2 Sensor node

The sensor node was designed to be a low-power device while keeping the cost as low as possible. The main components and features of the sensor node as follows:

- ESP32 Wrover-E microcontroller
- RA-02 LoRa module
- Three RJ-12 sensor sockets
- TDK NTCG163JF103FT1 NTC thermistor for environment temperature
- A socket for cellular network module to use in remote areas
- Battery connector for 18650 lithium-ion battery
- External power connector to use the node from a different power source than the battery
- HT7833 3,3V 500mA linear drop-out regulator
- 2N7002 MOSFETs for all power-consuming components
- STM809SW voltage supervisor to detect low battery level
- A push-button to wake up the module outside of its schedule

### 4.2.1 The parts selection

The main controller of the sensor node is ESP32 Wrover-E. The ESP32 microcontroller has WiFi and Bluetooth 4.1 connection features, suitable for low power applications[45]. Moreover, it is possible to cut down ESP32's power consumption to 10 $\mu$ A with deep sleep function.



Figure 23: ESP32 Wrover-E module[46]

Besides connectivity and low power features, ESP32 Wrover-E has the following features[45]:

- PCB antenna
- 4MB SPI flash
- 8MB Pseudo static RAM
- 240MHz Dual-core CPU

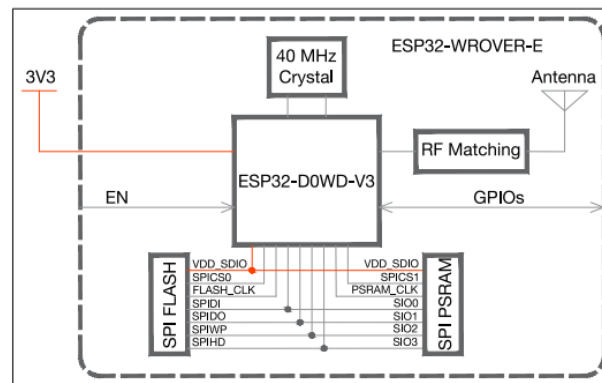


Figure 24: ESP32 Wrover-E block diagram[45]

In the sensor node, a LoRa radio module RA-02 from AI-Thinker was used. The RA-02 radio module is set to work on the EU433 band. The module is based on Semtech SX1278[47]. RA-02 features are:

- Receive sensitivity as low as -141dBm
- IPEX antenna connector
- Power consumption at 433MHz; for TX 93mA, for RX 12,15mA, for standby 1,6mA

While RA-02 has 1,6mA rated standby current, it is still a high value for the system. To save more power LoRa module's ground pin is manipulated by 2N7002 MOSFET. Therefore LoRa radio could be switched off completely when it is not used. The reason for selecting 2N7002 MOSFET is; 2N7002 is suitable for low power application, and it has 1,7 $\Omega$  drain to source resistance at 5V 500mA load[48].

The Ra-02 LoRa module and ESP32 Wrover-E connected via Serial Peripheral Interface(SPI) to the module.



Figure 25: Ra-02 LoRa radio module

Similar to LoRa radio's power off feature, all power-consuming components in the sensor node are controlled by a 2N7002 transistor. This includes three sensor connections, the external GPRS and LoRa radio.

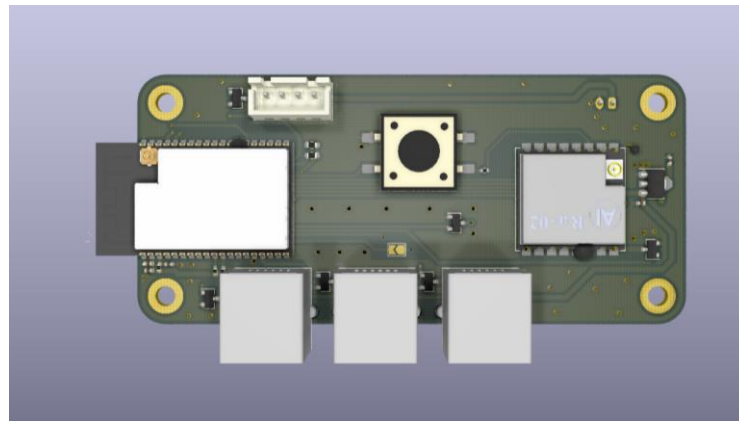


Figure 26: Sensor node front view on KiCAD

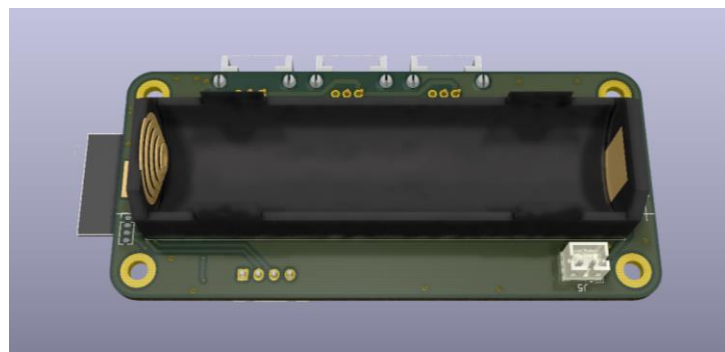


Figure 27: Sensor node back view on KiCAD

The dimensions of the sensor node from the WiFi antenna to the end edge of the PCB 94,6mm and width is 40mm.

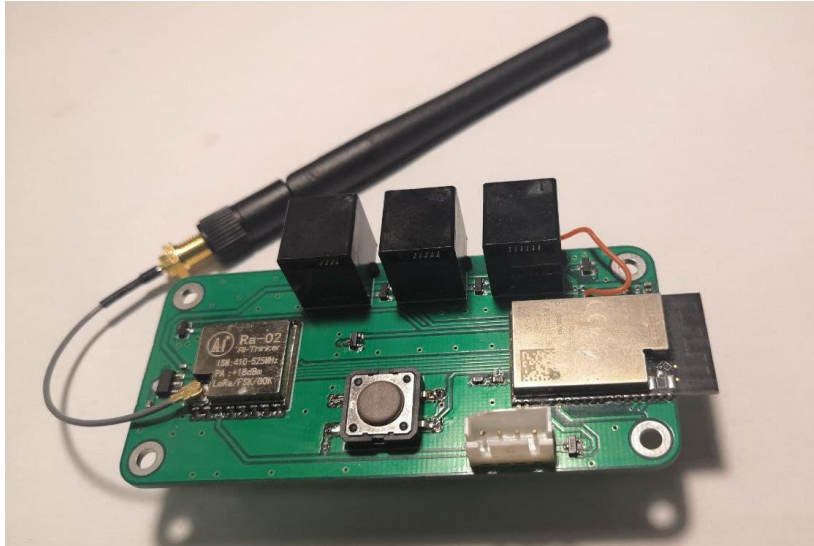


Figure 28: Sensor node

In addition to the sensor node, a programmer device was designed for the sensor node. The design of the programming circuit was taken from the ESP32 Wrover-E datasheet. The programming device features:

- USB Type C connection for power delivery and computer connection
- External power supply connector in case computer USB current is not enough
- LM1117 3.3V 1A linear drop-out regulator for sensor node voltage levels
- LEDs to show programming pins status
- Silicon Labs CP2102 based UART-USB converter
- Spring contacts for programming pins connection and power delivery to the sensor node

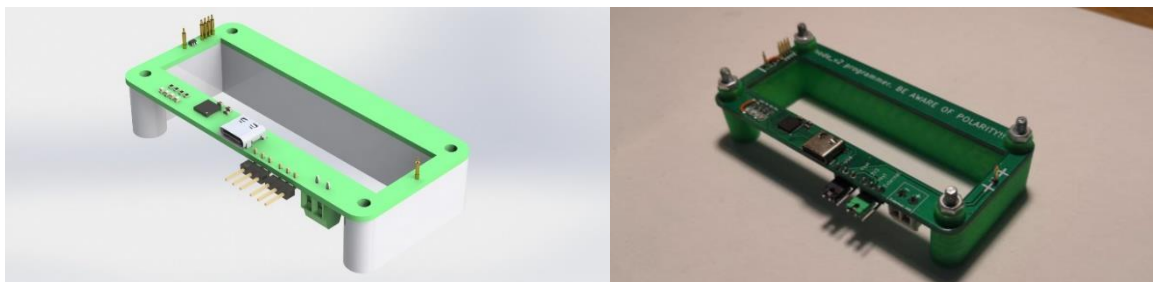


Figure 29: Sensor node programmer 3D model(on left), and assembled programmer(on right)

#### 4.2.2 Sensor node tests

The sensor node device was tested for LoRa communication range and battery drain.

##### Communication range test

In order to achieve maximum communication distance:

- LoRa signal TX power is set to the maximum of 17dB with a 3dBm antenna.
- During the test, two sensor nodes put at 2 meters height
- Spreading factor set to 12 and coding rate set to 4 to reduce noise

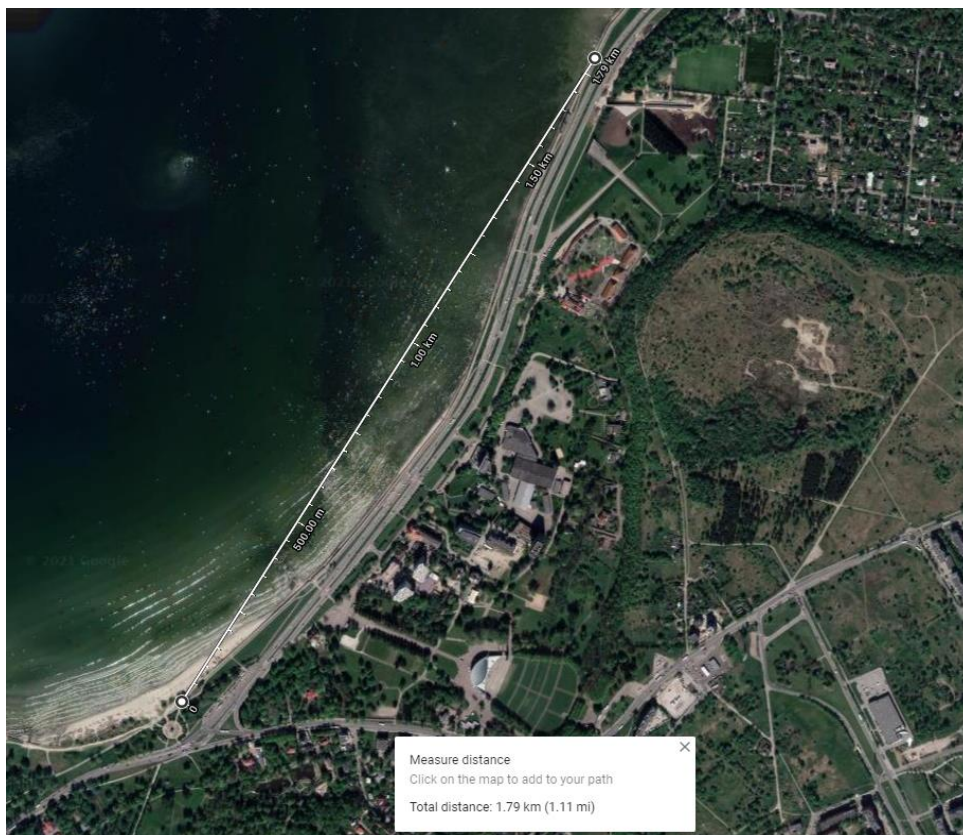


Figure 30: Range test in Pirita tee

The range test conducted along Pirita tee, Tallinn, and a maximum range of 1,79km with the minimum of -128 RSSI was achieved between the following coordinates:

- 59.44411539273833 N, 24.794022522014522 E
- 59.45777022742009 N, 24.810888251661076 E

## Battery life estimation

Battery consumption was kept at a minimum level for sensor node devices, both with hardware and software tweaks—all power drawing components and units controlled by MOSFET.

Component	On(mA)	Sleep(mA)	On duty cycle(%)	Sleep duty cycle(%)	mA/h
ESP32	300	0.15	0.13	99,87	0.539805
LoRa TX	12,5	0.01	0,11	99,89	0.113640
LoRa RX	95	0,01	0,2	99,8	0.199980
Sensor1	7.8	0.01	0.008	99.9917	0.000647
Sensor2	7.8	0.01	0.008	99.9917	0.000647
Sensor3	7.8	0.01	0.008	99.9917	0.000647
Path losses	3	0.01	0.13	99.87	0.003900
Total mA per hour					0,899
Estimated battery life for 3000mAh Lithium-ion battery					139 days

Table 8: Battery estimation

The battery life estimation was tested in a real-life scenario. In this scenario, two sensor nodes, each equipped with a 3000mAh battery and three I2C soil moisture sensors, were installed on the TalTech soccer field. According to the calculation in Table 6, the sensor node consumes 0,899mA per hour, and a 3000mAh battery should last 139 days. However, the test duration was one week. The consumption of 0,899mA per hour drains 95% of the 3000mAh battery, which means that a fully charged battery at 4,2V should be 4,06V at the end of a week. The test was conducted between 25/05/2021 at 20:34 and 01/06/2021 at 20:56. The measured battery at the end of the test was 4.034V, which is 86%.



Figure 31: Battery level after one week of test

A gateway installed on the side of the field and connected to the TalTech WiFi network. The locations of the sensors and the gateway are shown in Figure 31. The sensor nodes are colored in blue. The maximum distance from one sensor node to the gateway is 127m.

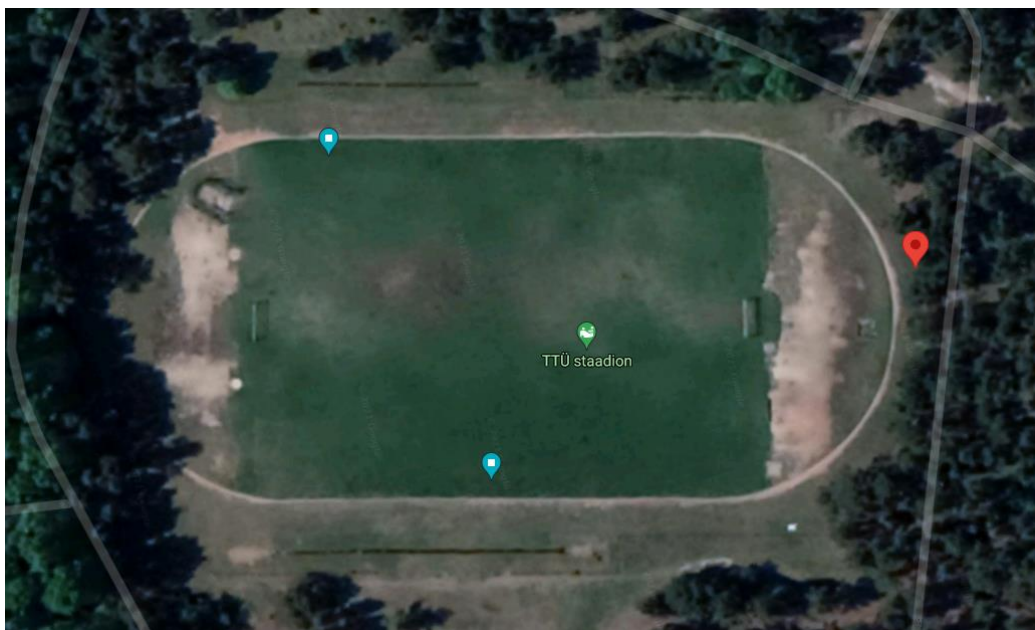


Figure 32: Sensor node and gateway location

### **Complete test of the system**

The sensor node cycled with four hours of intervals. In each cycle, data from three moisture sensors and environment temperature sensors were sent with LoRa, and this process took 3,8 seconds, followed by 15 seconds of gateway listening period. When the system awakes every 4 hours, the ESP32 Wrover-E powers on one sensor to gather data and then power-downs the sensor, this process was cycled for each sensor and

followed by reading the NTC thermistor for environment temperature and battery indicator. After all the reading processes were done, the LoRa radio wakes up and transmits the data to the gateway. After transmission, LoRa awaits the “data received” indicator from the gateway then continues with the sleep period. The “data received” feedback from the gateway to the sensor node includes a new setting parameter if available. The time window for the “data received” indicator on the sensor node side is 15 seconds. If the “data received” indicator was not arrived device sleeps for 1 minute and then wakes up for 15 seconds again. If the situation continues consecutively, the sleep time of one minute for the subsequent window increases. However, it is also visible from the gateway side in data collection problems from one node. The data flow chart is also represented in Figure33.

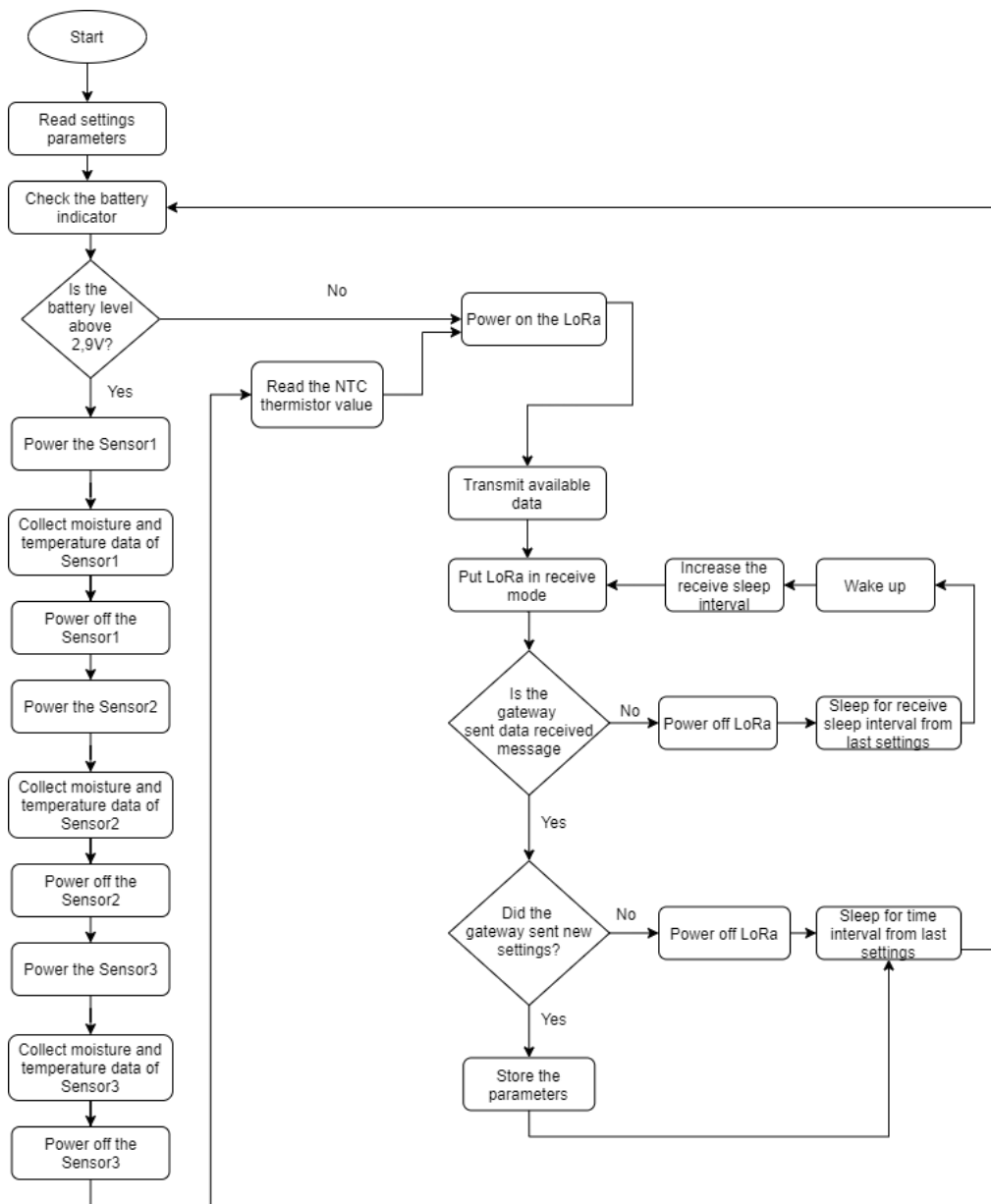


Figure 33: Sensor node data flow

The sensor node was enclosed in a 3D printed cover. The cover was made of 2 halving parts screwed together with the sensor node in the middle. The antenna was connected via IPEX to SMA cable where IPEX side connected to RA-02 LoRa module and SMA end mounted on the top half of the cover. The sensor node was placed at 40cm height from the ground. The sensor node assembly and its cover were done as in Figure34, and field installation was done as in Figure35.

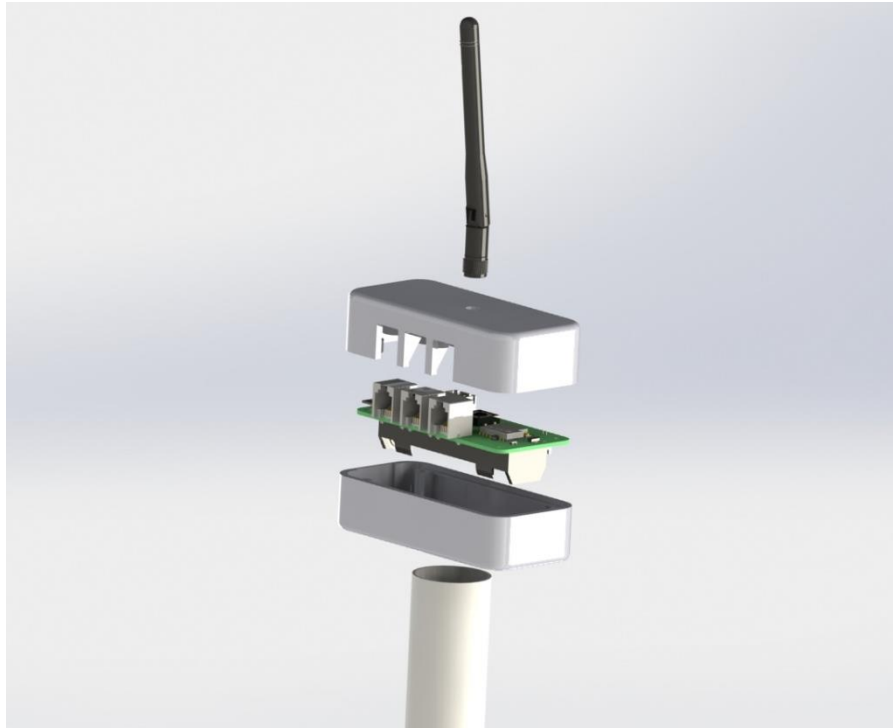


Figure 34: Sensor node assembly



Figure 35: Sensor node on the field

### 4.3 Web platform

The data collected from sensors uploaded to a cloud service for visualization. The web platform was based on open source map software kepler.gl. The map software enabled the combination of moisture data and NDVI data as layers on the map. The moisture levels were represented as hexagon tiles, and value increase represents color change and 3D hex blocks where its height is the value.



Figure 36:Moisture data on the map

The NDVI values were calculated from Sentinel-2 satellite data using Equation 12. The Moderate-resolution Imaging Spectroradiometer(MODIS) of Sentinel-2 was used as the source. For NIR, the B8-842nm and for R B4-665nm light bands were used[49]. The resolution of Sentinel-2 MODIS data in Figure 37 was 10 meters per pixel[49].

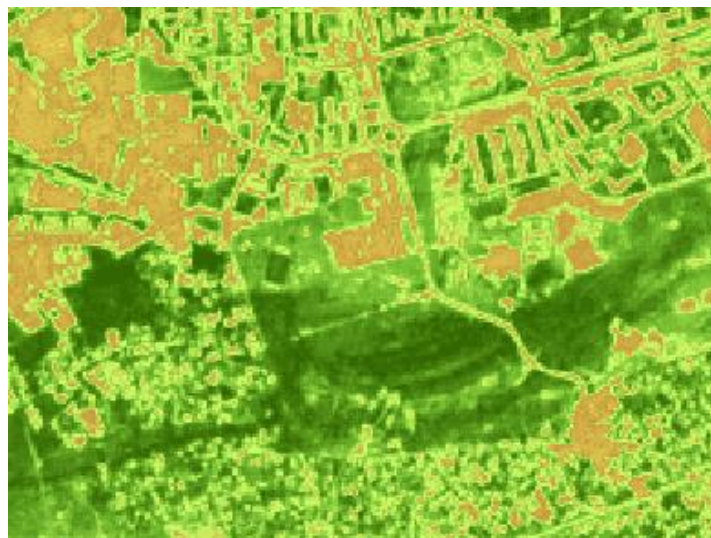


Figure 37:NDVI data of TalTech campus area from Sentinel2



Figure 38: Extracted region

The extracted region in Figure38 was transferred to the map software and combined with moisture data in Figure39.

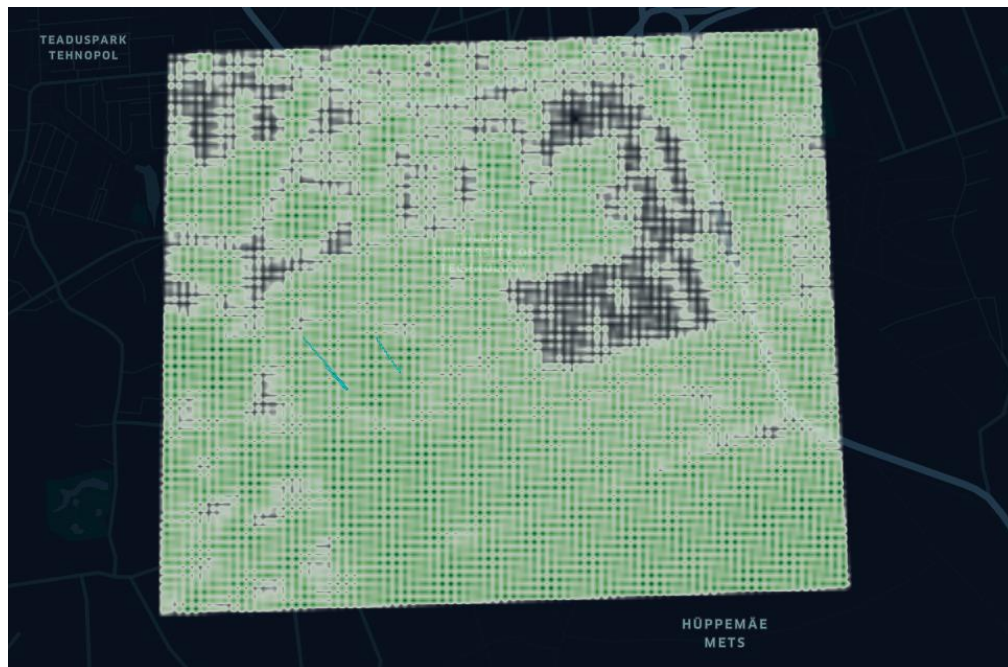


Figure 39: NDVI and moisture levels on map

## 5. DISCUSSION

The test results of three different sensors showed that the Catnip Electronics I2C moisture sensor performed better. The data from analog sensors were affected by their cable resistance. While the resistance of the cable had a direct effect on analog sensors, the I2C communication was also affected by cable length due to the capacitance of the cable. However, the issue on I2C was solved by lowering the I2C clock speed to 100Hz. The I2C communication was also beneficial for the microcontroller in the used GPIOs perspective. While each analog sensor requires a single pin for each sensor, the I2C sensors used the same communication lines

The I2C communication reliability could also be increased further by a shielded cable.

Even though the I2C sensor had the best performance, the price was at the same level as other sensors. The sensor manufactured by Catnip Electronics has an open-source design[44]. The open-source feature allowed to make changes in the circuit. The I2C sensor had light measurement and temperature measurement features. The light measurement circuit was removed to reduce the cost of the sensor, and the space from the light measurement part was removed; thus, PCB was shortened. As a result, the cost of the sensor was reduced to 2,88€.

Comparing Catnip Electronics I2C sensor and the I2C sensor manufactured for this thesis showed that the manufactured sensor did not show exact but similar responses. Therefore, it is assumed that the manufacturing vendor's PCB impedance and component supplier create the difference in measurements.

The sensor node battery consumption was performed to close the calculated values. While the calculation for one week of consumption showed that 5% of battery power should be used, the actual consumption was 9%. This extra consumption was due to the software cycle of the sensor node. As shown in the Figure33 flow chart, the LoRa radio of the device waits for the "data received" signal and repeats in incrementing cycles until data is received. The final data in Appendix 2 shows that the sensor node did not get a "data received" signal from the gateway on every cycle. The consumption from this waiting period could be reduced by saving the sensors' data into the flash memory of ESP32 Wrover-E and sending the data on the next wake-up opportunity. Apart from signal receive window consumption, the overall consumption could be reduced further with a better LDO and tweaking the deep sleep features of ESP32 Wrover-E.

The web platform was based on map software. It is visually enough to show data about the field with layers, and it is beneficial to add additional different datasets. The resolution of Sentinel-2 MODIS NDVI data used in Figure 37 was coarse. It could be improved by using commercial imaging solutions with lower meters per pixel resolution. It would also be beneficial to use additional indices together with NDVI.

## **6. CONCLUSION**

In the scope of this thesis, a satellite-assisted IoT soil irrigation monitoring system was developed. The system consisted of sensors, LoRa sensor nodes, and a web platform. Design and testing phases were completed on the planned schedule. As a result, the devices and a web platform were produced, and the thesis objectives were completed.

The manipulation of an open-source sensor design helped to reduce sensor costs of the system by 73%—the calculated theoretical battery lifetime achieved by 91% precision. In addition, the web platform successfully visualized the moisture data and NDVI data.

The web platform, in its current state, visualizes data sets by layer. For future work, the web platform was made to accept different datasets. Additionally, by implementing a smart water valve as an irrigation and fertilizer control system and combining current moisture sensing and NDVI data, the system could provide closed-loop control. Such a system would try to reach a crop yield by taking two inputs from NDVI data sets and moisture data and give output for watering and fertilizing.

In conclusion, the satellite-assisted IoT soil irrigation monitoring system was designed and prototyped. As the results of the performed tests, the monitoring system worked as expected in the real-life field test scenario. The system provides remote monitoring feature for the farmers who requires moderate and precise data about the agriculture field.

## 7. KOKKUVÕTE EESTI KEELES

Selle lõputöö raames töötati välja satelliitide abil toimuv IoT mulla niisutamise seiresüsteem. Süsteem koosnes anduritest, LoRa anduri sõlmedest ja veebiplatvormist. Projekteerimise ja testimise etapid viidi lõpule kavandatud ajakava järgi. Selle tulemusena toodeti seadmed ja veebiplatvorm ning lõputöö eesmärgid viidi lõpule.

Avatud lähtekoodiga anduri disainiga manipuleerimine aitas süsteemi andurikulusid vähendada 73% - arvutatud teoreetiline eluiga on saavutatud 91% täpsusega. Lisaks visualiseeris veebiplatvorm edukalt niiskuse andmed ja NDVI andmed.

Veebiplatvorm visualiseerib praeguses olekus andmekogumeid kihtide kaupa. Edasiseks tööks tehti veebiplatvorm erinevate andmekogumite aktsepteerimiseks. Lisaks, rakendades nutika veeventiili niisutamise ja väetise juhtimissüsteemina ning ühendades praegused niiskustundlikud ja NDVI andmed, võiks süsteem pakkuda suletud ahelaga juhtimist. Selline süsteem püüaks saavutada saagikuse, võttes NDVI andmekogumitest ja niiskuse andmetest kaks sisendit ning andes väljundi kastmiseks ja väetamiseks.

Kokkuvõtteks võib öelda, et satelliidi abil toimuv IoT mulla niisutamise seiresüsteem on välja töötatud ja on loodud prototüüp. Tehtud testide tulemustena toimis seiresüsteem reaalse välja katsetamise stsenaariumi korral ootuspäraselt. Süsteem pakub kaugseire funktsiooni põllumajandustootjatele, kes vajavad mõõdukaid ja täpseid andmeid põllumajanduse kohta.

## LIST OF REFERENCES

- [1] FAO, "FAOSTAT," 2017. <http://www.fao.org/faostat/en/#data> (accessed Oct. 09, 2020).
- [2] J. Mateo-Sagasta, S. Z. Marjani, and H. Turrall, "No Title," 2017. <http://www.fao.org/3/a-i7754e.pdf> (accessed Oct. 09, 2020).
- [3] D. B. Lobell, "The use of satellite data for crop yield gap analysis," *F. Crop. Res.*, vol. 143, pp. 56–64, Mar. 2013, doi: 10.1016/j.fcr.2012.08.008.
- [4] A. Berger, G. Ettlín, C. Quincke, and P. Rodríguez-Bocca, "Predicting the Normalized Difference Vegetation Index (NDVI) by training a crop growth model with historical data," *Comput. Electron. Agric.*, vol. 161, pp. 305–311, Jun. 2019, doi: 10.1016/j.compag.2018.04.028.
- [5] J. L. Hatfield, A. A. Gitelson, J. S. Schepers, and C. L. Walthall, "Application of Spectral Remote Sensing for Agronomic Decisions," *Celebr. Centen.*, vol. 100, no. S3, pp. 117–131, 2008, [Online]. Available: <https://doi.org/10.2134/agronj2006.0370c>.
- [6] J. Peng *et al.*, "A roadmap for high-resolution satellite soil moisture applications – confronting product characteristics with user requirements," *Remote Sensing of Environment*, vol. 252. Elsevier Inc., p. 112162, Jan. 01, 2020, doi: 10.1016/j.rse.2020.112162.
- [7] H. H. Nguyen, H. Kim, and M. Choi, "Evaluation of the soil water content using cosmic-ray neutron probe in a heterogeneous monsoon climate-dominated region," *Adv. Water Resour.*, vol. 108, pp. 125–138, Oct. 2017, doi: 10.1016/j.advwatres.2017.07.020.
- [8] I. Yolcubal, M. L. Brusseau, J. F. Artiola, P. J. Wierenga, and L. G. Wilson, "Environmental Physical Properties and Processes," in *Environmental Monitoring and Characterization*, Elsevier Inc., 2004, pp. 207–239.
- [9] J. Ding and R. Chandra, "Towards Low Cost Soil Sensing Using Wi-Fi," 2019, doi: 10.1145/3300061.3345440.
- [10] M. R. Mahmoudzadeh Ardekani, "Off- and on-ground GPR techniques for field-scale soil moisture mapping," *Geoderma*, vol. 200–201, pp. 55–66, Jun. 2013, doi: 10.1016/j.geoderma.2013.02.010.

- [11] K. Wu *et al.*, "A new drone-borne GPR for soil moisture mapping," *Remote Sens. Environ.*, vol. 235, p. 111456, Dec. 2019, doi: 10.1016/j.rse.2019.111456.
- [12] D. Nielsen and A. Johnson, "Ground Water and Vadose Zone Monitoring," in *Ground Water and Vadose Zone Monitoring*, West Conshohocken, PA, 1990, p. 40.
- [13] M. Razzaghmanesh and M. Borst, "Monitoring the performance of urban green infrastructure using a tensiometer approach," *Sci. Total Environ.*, vol. 651, pp. 2535–2545, Feb. 2019, doi: 10.1016/j.scitotenv.2018.10.120.
- [14] J. Mendes and D. Gallipoli, "Comparison of high capacity tensiometer designs for long-term suction measurements," *Phys. Chem. Earth*, vol. 115, p. 102831, Feb. 2020, doi: 10.1016/j.pce.2019.102831.
- [15] X. Deng *et al.*, "A calibration-free capacitive moisture detection method for multiple soil environments," *Meas. J. Int. Meas. Confed.*, p. 108599, Oct. 2020, doi: 10.1016/j.measurement.2020.108599.
- [16] A. Valente, R. Morais, A. Tuli, J. W. Hopmans, and G. J. Kluitenberg, "Multi-functional probe for small-scale simultaneous measurements of soil thermal properties, water content, and electrical conductivity," *Sensors Actuators, A Phys.*, vol. 132, no. 1 SPEC. ISS., pp. 70–77, Nov. 2006, doi: 10.1016/j.sna.2006.05.010.
- [17] GSMA, "3GPP Low Power Wide Area Technologies," 2016. [Online]. Available: <https://www.gsma.com/iot/wp-content/uploads/2016/10/3GPP-Low-Power-Wide-Area-Technologies-GSMA-White-Paper.pdf>.
- [18] "Sigfox Documentation." <https://support.sigfox.com/docs/how-to-test-in-production> (accessed Jan. 03, 2021).
- [19] C. Fournet and B. Ponsard, "An introduction to Sigfox radio system," in *LPWAN Technologies for IoT and M2M Applications*, Elsevier, 2020, pp. 103–118.
- [20] K. Mekki, E. Bajic, F. Chaxel, and F. Meyer, "A comparative study of LPWAN technologies for large-scale IoT deployment," *ICT Express*, vol. 5, no. 1, pp. 1–7, Mar. 2019, doi: 10.1016/j.icte.2017.12.005.
- [21] Semtec, "Semtech SX1276." <https://www.semtech.com/products/wireless-rf/lora-transceivers/sx1276> (accessed Jan. 03, 2021).

- [22] N. Ida, *Engineering electromagnetics*. 2000.
- [23] J. Hrisko, "Capacitive Soil Moisture Sensor Theory, Calibration, and Testing," *Maker Portal LLC*, 2020.
- [24] D. G. Archer and P. Wang, "The Dielectric Constant of Water and Debye-Hückel Limiting Law Slopes," *J. Phys. Chem. Ref. Data*, vol. 19, no. 2, pp. 371–411, Mar. 1990, doi: 10.1063/1.555853.
- [25] A. Martinez and A. P. Byrnes, "Modeling Dielectric-constant values of Geologic Materials: An Aid to Ground-Penetrating Radar Data Collection and Interpretation," *Curr. Res. Earth Sci.*, vol. 247, Jan. 2002.
- [26] M. A. Ertürk, M. A. Aydin, T. Büyükakkaşlar, and H. Evirgen, "A Survey on LoRaWAN Architecture, Protocol and Technologies," *Futur. Internet*, vol. 11, p. 216, Oct. 2019, doi: 10.3390/fi11100216.
- [27] M. F. A. Khan, "Lora Based Smart Agriculture System," Tallinn University of Technology, 2018.
- [28] Semtech Corporation, "LoRa Modulation Basics," 2015. [https://lora-developers.semtech.com/uploads/documents/files/Coexistence\\_of\\_LoRaWAN\\_and\\_UHF\\_RFID\\_Final\\_v3.pdf](https://lora-developers.semtech.com/uploads/documents/files/Coexistence_of_LoRaWAN_and_UHF_RFID_Final_v3.pdf) (accessed May 07, 2021).
- [29] M. Abu-Rgheff, "Fundamentals of Spread-Spectrum Techniques," 2007, pp. 153–194.
- [30] M. Viswanathan, *Digital Modulations using Matlab : Build Simulation Models from Scratch*. Independently published, 2017.
- [31] O. Rioul and J. C. Magossi, "On Shannon's Formula and Hartley's Rule: Beyond the Mathematical Coincidence," *Entropy*, vol. 16, no. 9. 2014, doi: 10.3390/e16094892.
- [32] و. قلخاني منوچهر, حيرانى علي, "Chirp Signal – FFT & PSD in Matlab & Python," 1390. <https://www.gaussianwaves.com/2014/07/chirp-signal-frequency-sweeping-fft-and-power-spectral-density-matlab-python/> (accessed Jun. 06, 2021).
- [33] E. Gambi, L. Montanini, D. Pigni, G. Ciattaglia, and S. Spinsante, "A home automation architecture based on LoRa technology and Message Queue Telemetry Transfer protocol," *Int. J. Distrib. Sens. Networks*, vol. 14, p. 155014771880683, Oct. 2018, doi: 10.1177/1550147718806837.

- [34] Y. Li, D. Li, W. Cui, and R. Zhang, "Research based on OSI model," in *2011 IEEE 3rd International Conference on Communication Software and Networks*, 2011, pp. 554–557, doi: 10.1109/ICCSN.2011.6014631.
- [35] H. Fang and S. B. T.-R. M. in E. S. and E. S. Liang, "Leaf Area Index Models☆," Elsevier, 2014.
- [36] Nasa, "Measuring Vegetation (NDVI & EVI)."  
[https://earthobservatory.nasa.gov/features/MeasuringVegetation/measuring\\_vegetation\\_2.php](https://earthobservatory.nasa.gov/features/MeasuringVegetation/measuring_vegetation_2.php) (accessed Jun. 04, 2021).
- [37] Y. Yigini, L. Montanarella, and P. Panagos, "European Contribution Towards a Global Assessment of Agricultural Soil Organic Carbon Stocks," in *Advances in Agronomy*, vol. 142, Academic Press Inc., 2017, pp. 385–410.
- [38] "Normalized Difference Vegetation Index."  
<https://land.copernicus.eu/global/products/ndvi> (accessed Jun. 03, 2021).
- [39] "Gravity: Analog Capacitive Soil Moisture Sensor- Corrosion Resistant."  
<https://www.dfrobot.com/product-1385.html> (accessed Jun. 05, 2021).
- [40] "Capacitive moisture sensor SK."  
[https://wiki.dfrobot.com/Capacitive\\_Soil\\_Moisture\\_Sensor\\_SKU\\_SEN0193](https://wiki.dfrobot.com/Capacitive_Soil_Moisture_Sensor_SKU_SEN0193) (accessed Jun. 06, 2021).
- [41] "TLC555 LinCMOS™ Timer."  
<https://www.ti.com/lit/ds/symlink/tlc555.pdf?ts=1622908644097>.
- [42] "SoilWatch 10 – Soil moisture sensor." <https://pino-tech.eu/product/soilwatch-10/> (accessed Jun. 05, 2021).
- [43] Pino-Tech, "Soilwatch 10." <https://pino-tech.eu/wp-content/uploads/2017/08/SoilWatch10.pdf> (accessed Jun. 06, 2021).
- [44] "I2C Soil moisture sensor." <https://www.tindie.com/products/miceuz/i2c-soil-moisture-sensor/> (accessed Jun. 06, 2021).
- [45] Espressif, "ESP32-WROVER-E & ESP32-WROVER-IE Datasheet," 2021.  
[https://www.espressif.com/sites/default/files/documentation/esp32-wrover-e\\_esp32-wrover-ie\\_datasheet\\_en.pdf](https://www.espressif.com/sites/default/files/documentation/esp32-wrover-e_esp32-wrover-ie_datasheet_en.pdf) (accessed Jun. 07, 2021).
- [46] "ESP32-WROVER-E (8MB)." <https://www.digikey.lt/product-detail/en/espressif->

systems/ESP32-WROVER-E-8MB/1965-ESP32-WROVER-E-8MB-CT-ND/11613165 (accessed Jun. 07, 2021).

- [47] "RA-02 LoRa module." [https://docs.air-thinker.com/\\_media/lora/docs/c048ps01a1\\_ra-02\\_product\\_specification\\_v1.1.pdf](https://docs.air-thinker.com/_media/lora/docs/c048ps01a1_ra-02_product_specification_v1.1.pdf) (accessed Jun. 07, 2021).
  
- [48] T.- Ab, "2N7000 2N7002 NDF7000A NDS7002A N-Channel Enhancement Mode Field Effect Transistor N-Channel Enhancement Mode Field Effect Transistor," 1995. <https://www.onsemi.com/pdf/datasheet/nds7002a-d.pdf> (accessed Jun. 07, 2021).
  
- [49] "Sentinel2 - Spatial Resolution." <https://sentinels.copernicus.eu/web/sentinel/user-guides/sentinel-2-msi/resolutions/spatial> (accessed Jun. 09, 2021).



## APPENDIX 2

Sensor	Lat	Long	Date	Value	Percentage
s1_3	59.39363	24.66547	25/05/2021 20:34	509	39.36
s1_2	59.39363	24.66544	25/05/2021 20:34	514	41.13
s1_1	59.39362	24.66548	25/05/2021 20:34	573	62.06
s2_1	59.39346	24.66423	25/05/2021 21:17	489	32.27
s2_2	59.39346	24.6642	25/05/2021 21:17	502	36.88
s2_3	59.39348	24.66423	25/05/2021 21:17	492	33.33
s1_3	59.39363	24.66547	26/05/2021 00:35	513	40.78
s1_2	59.39363	24.66544	26/05/2021 00:35	518	42.55
s1_1	59.39362	24.66548	26/05/2021 00:35	579	64.18
s2_1	59.39346	24.66423	26/05/2021 01:19	490	32.62
s2_2	59.39346	24.6642	26/05/2021 01:19	503	37.23
s2_3	59.39348	24.66423	26/05/2021 01:19	499	35.82
s1_3	59.39363	24.66547	26/05/2021 04:34	516	41.84
s1_2	59.39363	24.66544	26/05/2021 04:34	518	42.55
s1_1	59.39362	24.66548	26/05/2021 04:34	586	66.67
s2_1	59.39346	24.66423	26/05/2021 05:18	492	33.33
s2_2	59.39346	24.6642	26/05/2021 05:18	510	39.72
s2_3	59.39348	24.66423	26/05/2021 05:18	505	37.94
s1_3	59.39363	24.66547	26/05/2021 08:34	515	41.49
s1_2	59.39363	24.66544	26/05/2021 08:34	518	42.55
s1_1	59.39362	24.66548	26/05/2021 08:34	579	64.18
s2_1	59.39346	24.66423	26/05/2021 09:20	518	42.55
s2_2	59.39346	24.6642	26/05/2021 09:20	523	44.33
s2_3	59.39348	24.66423	26/05/2021 09:20	545	52.13
s1_3	59.39363	24.66547	26/05/2021 12:35	522	43.97
s1_2	59.39363	24.66544	26/05/2021 12:35	523	44.33
s1_1	59.39362	24.66548	26/05/2021 12:35	588	67.38
s2_1	59.39346	24.66423	26/05/2021 13:25	540	50.35
s2_2	59.39346	24.6642	26/05/2021 13:25	551	54.26
s2_3	59.39348	24.66423	26/05/2021 13:25	565	59.22
s1_3	59.39363	24.66547	26/05/2021 16:35	518	42.55
s1_2	59.39363	24.66544	26/05/2021 16:35	515	41.49
s1_1	59.39362	24.66548	26/05/2021 16:35	576	63.12
s2_1	59.39346	24.66423	26/05/2021 17:20	539	50
s2_2	59.39346	24.6642	26/05/2021 17:20	552	54.61
s2_3	59.39348	24.66423	26/05/2021 17:20	560	57.45
s1_3	59.39363	24.66547	26/05/2021 20:35	513	40.78
s1_2	59.39363	24.66544	26/05/2021 20:35	510	39.72
s1_1	59.39362	24.66548	26/05/2021 20:35	576	63.12
s2_1	59.39346	24.66423	26/05/2021 21:21	538	49.65
s2_2	59.39346	24.6642	26/05/2021 21:21	550	53.9

s2_3	59.39348	24.66423	26/05/2021 21:21	559	57.09
s1_3	59.39363	24.66547	27/05/2021 00:36	535	48.58
s1_2	59.39363	24.66544	27/05/2021 00:36	543	51.42
s1_1	59.39362	24.66548	27/05/2021 00:36	625	80.5
s2_1	59.39346	24.66423	27/05/2021 01:22	526	45.39
s2_2	59.39346	24.6642	27/05/2021 01:22	550	53.9
s2_3	59.39348	24.66423	27/05/2021 01:22	559	57.09
s1_3	59.39363	24.66547	27/05/2021 04:36	548	53.19
s1_2	59.39363	24.66544	27/05/2021 04:36	552	54.61
s1_1	59.39362	24.66548	27/05/2021 04:36	655	91.13
s2_1	59.39346	24.66423	27/05/2021 05:23	525	45.04
s2_2	59.39346	24.6642	27/05/2021 05:23	552	54.61
s2_3	59.39348	24.66423	27/05/2021 05:23	566	59.57
s1_3	59.39363	24.66547	27/05/2021 08:36	495	34.4
s1_2	59.39363	24.66544	27/05/2021 08:36	502	36.88
s1_1	59.39362	24.66548	27/05/2021 08:36	551	54.26
s2_1	59.39346	24.66423	27/05/2021 09:22	548	53.19
s2_2	59.39346	24.6642	27/05/2021 09:22	552	54.61
s2_3	59.39348	24.66423	27/05/2021 09:22	655	91.13
s1_3	59.39363	24.66547	27/05/2021 12:37	498	35.46
s1_2	59.39363	24.66544	27/05/2021 12:37	502	36.88
s1_1	59.39362	24.66548	27/05/2021 12:37	554	55.32
s2_1	59.39346	24.66423	27/05/2021 13:22	518	42.55
s2_2	59.39346	24.6642	27/05/2021 13:22	515	41.49
s2_3	59.39348	24.66423	27/05/2021 13:22	576	63.12
s1_3	59.39363	24.66547	27/05/2021 16:35	498	35.46
s1_2	59.39363	24.66544	27/05/2021 16:35	501	36.52
s1_1	59.39362	24.66548	27/05/2021 16:35	550	53.9
s2_1	59.39346	24.66423	27/05/2021 17:21	520	43.26
s2_2	59.39346	24.6642	27/05/2021 17:21	552	54.61
s2_3	59.39348	24.66423	27/05/2021 17:21	563	58.51
s1_3	59.39363	24.66547	27/05/2021 20:34	506	38.3
s1_2	59.39363	24.66544	27/05/2021 20:34	505	37.94
s1_1	59.39362	24.66548	27/05/2021 20:34	559	57.09
s2_1	59.39346	24.66423	27/05/2021 21:17	518	42.55
s2_2	59.39346	24.6642	27/05/2021 21:17	523	44.33
s2_3	59.39348	24.66423	27/05/2021 21:17	545	52.13
s1_3	59.39363	24.66547	28/05/2021 00:35	512	40.43
s1_2	59.39363	24.66544	28/05/2021 00:35	507	38.65
s1_1	59.39362	24.66548	28/05/2021 00:35	564	58.87
s2_1	59.39346	24.66423	28/05/2021 01:19	518	42.55
s2_2	59.39346	24.6642	28/05/2021 01:19	523	44.33
s2_3	59.39348	24.66423	28/05/2021 01:19	545	52.13
s1_3	59.39363	24.66547	28/05/2021 04:34	513	40.78
s1_2	59.39363	24.66544	28/05/2021 04:34	508	39.01

s1_1	59.39362	24.66548	28/05/2021 04:34	568	60.28
s2_1	59.39346	24.66423	28/05/2021 05:18	509	39.36
s2_2	59.39346	24.6642	28/05/2021 05:18	514	41.13
s2_3	59.39348	24.66423	28/05/2021 05:18	563	58.51
s1_3	59.39363	24.66547	28/05/2021 08:34	507	38.65
s1_2	59.39363	24.66544	28/05/2021 08:34	501	36.52
s1_1	59.39362	24.66548	28/05/2021 08:34	559	57.09
s2_1	59.39346	24.66423	28/05/2021 09:20	520	43.26
s2_2	59.39346	24.6642	28/05/2021 09:20	539	50
s2_3	59.39348	24.66423	28/05/2021 09:20	565	59.22
s1_3	59.39363	24.66547	28/05/2021 12:35	498	35.46
s1_2	59.39363	24.66544	28/05/2021 12:35	495	34.4
s1_1	59.39362	24.66548	28/05/2021 12:35	520	43.26
s2_1	59.39346	24.66423	28/05/2021 13:25	511	40.07
s2_2	59.39346	24.6642	28/05/2021 13:25	518	42.55
s2_3	59.39348	24.66423	28/05/2021 13:25	554	55.32
s1_3	59.39363	24.66547	28/05/2021 16:35	490	32.62
s1_2	59.39363	24.66544	28/05/2021 16:35	492	33.33
s1_1	59.39362	24.66548	28/05/2021 16:35	519	42.91
s2_1	59.39346	24.66423	28/05/2021 17:20	516	41.84
s2_2	59.39346	24.6642	28/05/2021 17:20	522	43.97
s2_3	59.39348	24.66423	28/05/2021 17:20	560	57.45
s1_3	59.39363	24.66547	28/05/2021 20:35	494	34.04
s1_2	59.39363	24.66544	28/05/2021 20:35	501	36.52
s1_1	59.39362	24.66548	28/05/2021 20:35	526	45.39
s2_1	59.39346	24.66423	28/05/2021 21:21	504	37.59
s2_2	59.39346	24.6642	28/05/2021 21:21	507	38.65
s2_3	59.39348	24.66423	28/05/2021 21:21	548	53.19
s1_3	59.39363	24.66547	29/05/2021 00:36	498	35.46
s1_2	59.39363	24.66544	29/05/2021 00:36	502	36.88
s1_1	59.39362	24.66548	29/05/2021 00:36	530	46.81
s2_1	59.39346	24.66423	29/05/2021 01:22	506	38.3
s2_2	59.39346	24.6642	29/05/2021 01:22	509	39.36
s2_3	59.39348	24.66423	29/05/2021 01:22	551	54.26
s1_3	59.39363	24.66547	29/05/2021 04:36	511	40.07
s1_2	59.39363	24.66544	29/05/2021 04:36	507	38.65
s1_1	59.39362	24.66548	29/05/2021 04:36	544	51.77
s2_1	59.39346	24.66423	29/05/2021 05:23	510	39.72
s2_2	59.39346	24.6642	29/05/2021 05:23	512	40.43
s2_3	59.39348	24.66423	29/05/2021 05:23	549	53.55